Thesis for the Degree of Doctor of Philosophy

Antenna Designs Aiming at the Next Generation of Wireless Communication

Sadegh Mansouri Moghaddam

CHALMERS

Department of Electrical Engineering
Communications, Antennas, and Optical Networks Division
Chalmers University of Technology

Göteborg, Sweden 2019

Antenna Designs Aiming at the Next Generation of Wireless Communication

Sadegh Mansouri Moghaddam

ISBN 978-91-7905-192-1

Doktorsavhandlingar vid Chalmers tekniska högskola
Ny serie nr 4659
ISSN 0346-718X

Department of Electrical Engineering
Communications, Antennas, and Optical Networks Division
Chalmers University of Technology
SE–412 96 Göteborg
Sweden
Telephone: +46 (0)31 – 772 1000
Email: sadegh.mansouri@chalmers.se

Typeset by the author using LaTeX.

Chalmers Reproservice
Göteborg, Sweden 2019

To my family

Abstract

Millimeter-wave (mm-wave) frequencies have drawn large attention, specifically for the fifth generation (5G) of wireless communication, due to their capability to provide high data-rates. However, design and characterization of the antenna system in wireless communication will face new challenges when we move up to higher frequency bands.

The small size of the components at higher frequencies will make the integration of the antennas in the system almost inevitable. Therefore, the individual characterization of the antenna can become more challenging compared to the previous generations. This emphasizes the importance of having a reliable, simple and yet meaningful Over-the-Air (OTA) characterization method for the antenna systems. To avoid the complexity of using a variety of propagation environments in the OTA performance characterization, two extreme or edge scenarios for the propagation channels are presented, i.e., the Rich Isotropic Multipath (RIMP) and Random Line-of-Sight (Random-LoS). MIMO efficiency has been defined as a Figure of Merit (FoM), based on the Cumulative Distribution Function (CDF) of the received signal, due to the statistical behavior of the signal in both RIMP and Random-LoS. Considering this approach, we have improved the design of a wideband antenna for wireless application based on MIMO efficiency as the FoM of the OTA characterization in a Random-LoS propagation environment. We have shown that the power imbalance and the polarization orthogonality plays major roles determining the 2-bitstream MIMO performance of the antenna in Random-LoS. In addition, a wideband dual-polarized linear array is designed for an OTA Random-LoS measurement set-up for automotive wireless systems.

The next generation of wireless communication is extended throughout multiple narrow frequency bands, varying within 20-70 GHz. Providing an individual antenna system for each of these bands may not be feasible in terms of cost, complexity and available physical space. Therefore, Ultra-Wideband (UWB) antenna arrays, covering multiple mm-wave frequency bands represent a versatile candidate for these antenna systems. In addition to having wideband characteristics, these antennas should offer an easy integration capability with the active modules. We present a new design of UWB planar arrays for mm-wave applications. The novelty is to propose planar antenna layouts to provide large bandwidth at mm-wave frequencies, using simplified standard PCB manufacturing techniques. The proposed antennas are based on

Tightly Coupled Dipole Arrays (TCDAs) concept with integrated feeding network.

Keywords: Millimeter-wave, 5G, OTA, RIMP, Random-LoS, MIMO efficiency, CDF, PoD, Ultra-Wideband (UWB) antenna, Phased array antenna, Tightly-Coupled Dipole Array (TCDA).

Preface

This thesis is in partial fulfillment for the degree of Doctor of Philosophy at Chalmers University of Technology, Gothenburg, Sweden.

The work resulting in this thesis was carried out between October 2014 and September 2019 at the Antenna Systems Group, Division of Communications, Antennas, and Optical Networks, Department of Electrical Engineering, Chalmers University of Technology. The late Professor Per-Simon Kildal (till April 2016) and Professor Jian Yang are the main supervisors and Professor Jian Yang is the examiner. In addition, Associate Professor Andrés Alayón Glazunov and Associate Professor Ashraf Uz Zaman are the co-supervisors.

The present work has partially been supported by the Swedish Governmental Agency for Innovation Systems (VINNOVA) within the VINN Excellence Center Chase at Chalmers, and by the same VINNOVA with a project on MIMO hardware within the Innovative ICT 2013 program. In addition, it is carried out within the Strategic Innovation Program "Smarter Electronics Systems", a joint venture of Vinnova, Formas and Energy Agency, with grant no. 2017-01881 and also by the financial support from H2020-MSCA-RISE-2017 is3DMIMO project, no. 734798.

Acknowledgment

Finishing this thesis would have not been possible without the continuous support and help of many individuals. I have enjoyed the help and company of many wonderful people during these five years and I'm not sure I will be able to properly thank them all.

First and foremost, I wish to express my deepest gratitude to my late supervisor Professor Per-Simon Kildal for giving me the opportunity to start my PhD in the antenna group at Chalmers. I've learned many lessons from him and I'm sure I will not be able to mention them all but most of all, the enthusiasm in life, kindness and respect. I can distinctly remember some of the moments I've experienced with him which I'm sure have changed me to become the person I am now. I would never forget his laughs derived by a pure joy specifically after seeing the video I made for the Christmas dinner and that was one of the happiest and most satisfying moments of my life. I would like to thank my supervisor Professor Jian Yang for his continuous support, patience and attention throughout the follow up of my study and I am deeply grateful for that. I would also like to thank my co-supervisor Associate Professor Andrés Alayón Glazunov for his valuable helps, feedbacks and guidance. Furthermore, I wish to thank Associate Professor Ashraf Uz Zaman for his interest, attention and time throughout the last year of my study. I would like to recognize the researchers which I had the opportunity to collaborate with, Associate Professor Vessen Vassilev, Assistant Professor Zhongxia Simon He and Associate Professors Tianling Zhang and Lei Chen. I also would like to acknowledge all the industrial partners, especially Mattias Gustafsson from Huawei Technologies Sweden, Astrid Algaba Brazález, Lars Manholm and Stefan Thöresson from Ericsson and Lars-Inge Sjöqvist and Thomas Emanuelsson from Gapwaves.

A huge thanks goes to my five years officemate, Madeleine, for bearing with me for such a long time and laughing at my unfunny jokes. I would also like to almost equally thank Carlo for all the fun and enjoyable moments we shared together. Thank you guys for helping me, especially in the past year and not giving up on me. A big thanks goes to Abbas for helping me to find this position at Chalmers and helping me before and after coming to Sweden. Thanks for all the laughs we shared. Thanks to all my friends in the antenna group for the friendly and enjoyable work environment and thanks for all the supports. I wish to particularly thank Astrid, Aidin, Wan-Chun, Jinlin, Oleg, Jonas, Navid and Artem. I would also like to thank the entire

group, the former and new students and seniors, as well as my colleagues at the Electrical Engineering department. Thanks to all my friends in Sweden, in particular, Samar, Ramin, Sina, Abolfazl, Pegah, Maryam, Parastoo, Sepideh, Tomas, Kamran, Max, Giuseppe, Cristina, Fatemeh and Mohammad for keeping me a great company, Thanks to Enzo. And a special thanks to Madeleine for proofreading this thesis.

The greatest thanks goes to my family for their continuous support and endless love. I'm sure you know that I wish you all the best and I'm grateful for everything you have given me.

This journey of five years has been rich with valuable experiences and unforgettable memories for me and I thank you all for that. In case the rest of the thesis is going to be boring for you, I suggest you to see the video by the link below, "it is worth it, it is really fun".

https://www.youtube.com/watch?v=AlKUjFiQt6Q

Sadegh
Göteborg, September 2019

List of Publications

This thesis is based on the work contained in the following appended papers:

Paper A
S. M. Moghaddam, A. A. Glazunov, P. -S. Kildal, J. Yang and M. Gustafsson, "Improvement of an octave bandwidth bowtie antenna design based on the analysis of a MIMO efficiency metric in Random-LOS", *Microwave and Optical Technology Letteres*, vol. 59, pp. 1229-1233, 2017.

Paper B
S. M. Moghaddam, A. A. Glazunov, J. Yang, "Wideband Dual-Polarized Linear Array Antenna For Random-LOS OTA Measurement", *IEEE Transactions on Antennas and Propagation*, vol. 66, no. 5, pp. 2365-2373, May 2018.

Paper C
S. M. Moghaddam, A. A. Glazunov, J. Yang and M. Gustafsson, "Semi-Omnidirectional Dual-Polarized Wideband Multiport Antennas for MIMO Applications in Random-LOS and RIMP", in *Proceedings of the 11th European Conference on Antennas and Propagation, EuCAP 2017* , Paris, France, March-April 2017.

Paper D
S. M. Moghaddam, J. Yang and A. U. Zaman, "Fully-Planar Ultra-Wideband Tightly-Coupled Array (FPU-TCA) with Integrated Feed for Wide-Scanning Millimeter-Wave Applications", under revision for *IEEE Transactions on Antennas and Propagation.*

Paper E
S. M. Moghaddam, A. U. Zaman, J. Yang and A. A. Glazunov, "Tightly-Coupled Aperture-Coupled Magneto-Electric Dipole for Millimeter-Wave Phased-Array Antenna", in *Proceedings of the 13th European Conference on Antennas and Propagation, EuCAP 2019* , Krakow, Poland, April 2019.

Paper F
S. M. Moghaddam, J. Yang and A. A. Glazunov, "A Planar Dual-Polarized Ultra-

Wideband Millimeter-Wave Array Antenna", in *Proceedings of the 12th European Conference on Antennas and Propagation, EuCAP 2018* , London, UK, April 2018.

Other related publications of the Author not included in this thesis:

1. P. -S. Kildal, **S. M. Moghaddam**, X. Chen, M. Gustafsson, and Z.Chen, "Correction to "MIMO Characterization on System Level of 5G Micro Base Stations Subject to Randomness in LOS", *IEEE Access*, vol. 3, pp. 3151-3152, 2015.

2. A. Razavi, A. A. Glazunov, **S. M. Moghaddam**, R. Maaskant, and J. Yang, "Characterization method of an automotive random-LOS OTA measurement setup", *Progress In Electromagnetics Research*, vol. 84, pp. 47-60, 2018.

3. T. Zhang, L. Chen, **S. M. Moghaddam**, A. U. Zaman, J. Yang, "Ultra-wideband Linearly Polarized Planar Bowtie Array Antenna with Feeding Network using Dielectric-based Inverted Microstrip Gap Waveguide", submitted to *IET Microwaves, Antennas and Propagation*.

4. **S. M. Moghaddam**, A. A. Glazunov, J. Yang, M. Gustafsson, and P. -S. Kildal, "Comparison of 2-bitstream polarization-mimo performance of 2 and 4-port bowtie antennas for LTE in Random-LOS", *2015 International Symposium on Antennas and Propagation (ISAP).*, pp. 1-4, Nov 2015.

5. **S. M. Moghaddam**, A. A. Glazunov, J. Yang, and P. -S. Kildal, "Double broadband balun structure using CRLH TL for differential excitation of dual-polarized self-grounded bow-tie antenna", *PIERS 2015*, pp. 1966-1970.

6. A. A. Glazunov, P. -S. Kildal, J. Carlsson, M. S. Kildal, and **S. Mansouri**, "Impact of the spatial user distribution on the coverage antenna pattern of Maximum Ratio Combining in Random Line-Of-Sight", in *Proceedings of the 9^{th} European Conference on Antennas and Propagation, EuCAP 2015* , Lisbon, Portugal, April 2015.

7. **S. M. Moghaddam**, P.-S. Kildal, A. A. Glazunov, and J. Yang, "Designing a dual-polarized octave bandwidth bowtie antenna for a linear array", in *Proceedings of the 10^{th} European Conference on Antennas and Propagation, EuCAP 2016* , Davos, Switzerland, April 2016.

8. A. A. Glazunov, **S. M. Moghaddam** "Zero-forcing MIMO efficiency in random line-of-sight", in *Proceedings of the 10^{th} European Conference on Antennas and Propagation, EuCAP 2016* , Davos, Switzerland, April 2016.

9. **S. M. Moghaddam**, P. -S. Kildal, A. A. Glazunov, J. Yang and M. Gustafsson, Â´Â´A self-grounded dual-polarized wideband bowtie with improved MIMO performance in Random-LOS", *2016 IEEE International Symposium on Antennas and Propagation (APSURSI).*, pp. 531-532, 2016.

10. A. A. Glazunov, **S. M. Moghaddam** and J. Yang, "Simulating the MIMO efficiency of antennas", *2017 International Symposium on Antennas and Propagation (ISAP).*, pp. 1-2, Nov 2017.

11. **S. M. Moghaddam**, J. Yang and A. A. Glazunov, "Ultra-wideband millimeter-wave bowtie antenna", *2017 International Symposium on Antennas and Propagation (ISAP).*, pp. 1-2, Nov 2017.

12. J. Yang, **S. M. Moghaddam**, A. U. Zaman, Z. S. He and V. Vassilev, "PCB Based UWB mm-Wave Smart Capped Bowtie Array for 5G Communication Systems", *2018 IEEE International Symposium on Antennas and Propagation (USNC/URSI) National Radio Science Meeting.*, pp. 631-632, 2018.

13. **S. M. Moghaddam**, J. Yang, A. A. Glazunov, and A. U. Zaman, "A Planar Single-Polarized Ultra-Wideband Antenna Element for Millimeter-Wave Phased Array", *2018 International Symposium on Antennas and Propagation (ISAP).*, pp. 1-2, Oct 2018.

14. T. Zhang, L. Chen, **S. M. Moghaddam**, A. U. Zaman and J. Yang, "Wideband Dual-polarized Array Antenna on Dielectric-based Inverted Microstrip Gap Waveguide", in *Proceedings of the 13th European Conference on Antennas and Propagation, EuCAP 2019* , Karakow, Poland, April 2019.

15. L. Chen, T. Zhang, **S. M. Moghaddam**, A. U. Zaman and J. Yang, "A Method of Reducing Mutual Coupling Using an Extra Coupling Path", in *Proceedings of the 13th European Conference on Antennas and Propagation, EuCAP 2019* , Karakow, Poland, April 2019.

16. M. Alibakhshikenari, **S. M. Moghaddam**, A. U. Zaman, J. Yang, B. S. Virdee and E. Limiti, "Wideband Sub-6 GHz Self-Grounded Bow-Tie Antenna with New Feeding Mechanism for 5G Communication Systems", in *Proceedings of the 13th European Conference on Antennas and Propagation, EuCAP 2019* , Karakow, Poland, April 2019.

17. T. Zhang, L. Chen, **S. M. Moghaddam**, A. U. Zaman, J. Yang, "Ultra-wideband Circularly Polarized Planar Array Antenna Using Single-Arm-Spiral Elements and Dielectric-based IMGW", accepted for *2019 International Symposium on Antennas and Propagation (ISAP)*, Xian, China, October-November 2019.

Acronyms

3GPP	3rd Generation Partnership Project
5G	Fifth Generation mobile networks
AoA	Angle of Arrival
AWGN	Additive White Gaussian Noise
CDF	Cumulative Distribution Function
CRLH	Composite Right Left Hand
CPS	Coplanar stripline
CSA	Current Sheet Array
CSI	Channel State Information
DUT	Device Under Test
EGC	Equal-Gain Combining
eMBB	enhanced Mobile Broadband
EMC	Electromagnetic Compatibility
FSS	Frequency Selective Surface
GER	Group Error Rate
IMT	International Mobile Telecommunications
IoT	Internet of Things
ITS	Intelligent Transportation Systems
LOS	Line Of Sight
LTE	Long-Term Evolution
LTCC	Low Temperature Cofired Ceramic
M2M	Machine to Machine
MBB	Mobile Broadband
MED	Magneto Electric Dipole
MIMO	Multiple-Input Multiple-Output
mMTC	massive Machine Type Communications
MRC	Maximal Ration Combining
NR	New Radio
OFDM	Orthogonal Frequency-Division Multiplexing
OTA	Over-The-Air

PCB	Printed Circuit Board
PoD	Probability of Detection
PUMA	Planar Ultra wideband Modular Array
Random-LOS	Random-Line of Sight
RIMP	Rich Isotropic Multipath
SC	Selection Combining
SIMO	Single-Input Multiple-Output
SISO	Single-Input Single-Output
SIW	Substrate Integrated Waveguide
SNR	Signal-to-Noise Ratio
SVD	Singular Value Decomposition
TCDA	Tightly-Coupled Dipole Array
TCDA-IB	Tightly-Coupled Dipole Array with Integrated Balun
TE	Transverse Electric
TIS	Total Isotropic Sensitivity
TM	Transverse Magnetic
TRP	Total Radiated Power
URLLC	Ultra-Reliable Low-Latency Communications
UWB	Ultra-Wideband
XPD	Cross-polar Power Discrimination
ZF	Zero-Forcing

Contents

Part I

Introductory Chapters

Chapter 1

Introduction

The continues growth of wireless communication in past years has called for various user and application trends [1–3]. This includes: ultra-low latency and high reliability communications, in which users expect to experience instantaneous connectivity in applications such as cloud services and virtual/augmented realities. Also, automated cars, traffic control optimization, smart grid and e-health are other examples of machine-centric communication which requires low-latency and hight reliability. Another user trend for next generation of wireless communication is to support large number of dense users, e.g., users in public transportations or large stadium, and machine-to-machine (M2M) communication in traffic jams. Maintaining the high quality of communication at high mobility is another expected feature for future wireless communication. Also, application trends for the upcoming wireless communication can extend to enhanced multimedia services which will lead to a demand for significantly high date rate communication. And finally in the future, objects which can benefit from interconnections, such as smart phones, cameras, vehicles, sensors and etc. are expected to be connected. Therefore, the number of the connected devices will increase significantly due to the advent of Internet of Things (IoT).

Although the requirements for the fifth generation (5G) of wireless communication is yet to be finalized, the three main expected usage scenarios can be envisioned as: enhanced Mobile Broadband (eMBB), Ultra-Reliable Low Latency Communications (URLLC) and massive Machine Type Communications (mMTC) [2]. Mobile Broadband (MBB) refers to the human centric use cases for access to multimedia, services and data. The continuous increasing support of MBB through improved peak/average/cell-edge data rates, increased capacity for hotspots i.e., areas with dense users, and improved coverage for wide areas with medium to high mobilities are addressed as eMBB. URLLC introduces strict requirements in terms of latency and availability for emerging critical applications such as industrial internet, smart grids, infrastructure protection, remote surgery and intelligent transportation systems (ITSs). And at last, mMTC is necessary to support the envisioned 5G IoT

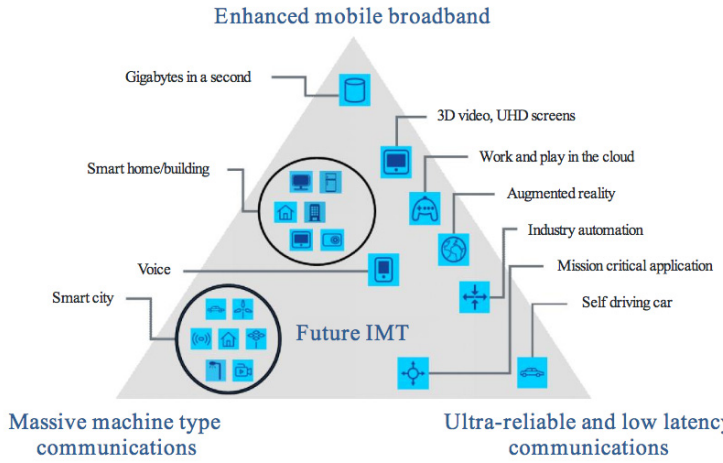

Figure 1.1: Usage scenarios of IMT for 2020 and beyond [2].

scenario with very large number of connected devices with low cost and long battery life requirements. These three main usage scenarios are depicted in Fig. 1.1.

Two tracks have been suggested to make up the 5G radio access roadmap in 3GPP [1], one is based on the evolution of LTE and the other is called New Radio (NR) access. LTE-5G can provide as many 5G requirements and use cases as possible and investors in LTE do not need to be concerned about their previous investments. However, it is restricted mainly due to the limited available spectrum. On the other hand, the NR-5G does not need any compatibility requirements related to the previous generations and therefore can introduce more fundamental changes including the usage of millimeter-Wave (mm-Wave) frequencies.

Despite all these new compelling advantages, making use of the next generation wireless communication will introduce many new challenges. In general, these challenges can be categorized into two main categories; the ones related to the implementation of the system and the ones introduced by the evaluation of the implemented system. In the following sections we try to explain and identify some of these challenges, mostly related to the antenna design approach.

1.1 System Implementation

A typical architecture of the mobile network is shown in Fig. 1.2. It consists of three main parts, the mobile fronthaul/Access, the backhaul and the mobile core. The mobile front end interfacing part of the cellular network is known as mobile fronthaul. It interfaces the end users with the rest of the network through base stations and macro cells. The back end part of the cellular network which connects

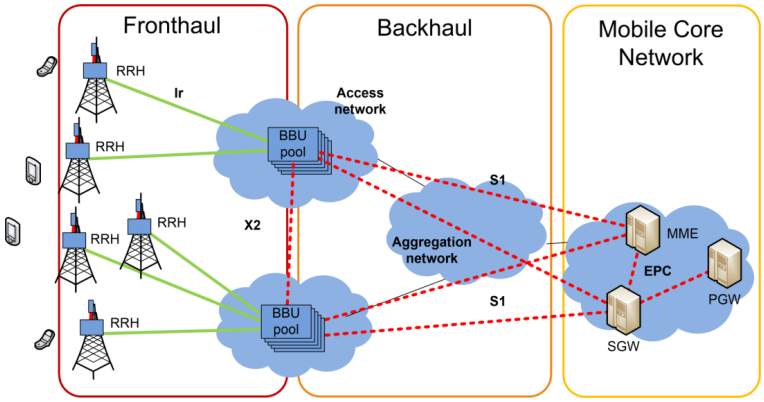

Figure 1.2: Fronthaul transport network [5].

the fronthaul to the mobile core network is called backhaul, which houses baseband units and aggregation networks. However in [4], an alternative architecture called Xhaul is proposed which aims to develop a 5G integrated backhaul and fronthaul transport network.

The mobile cores are linked to each other and to the backhaul by optical fibers, due to fiber's higher capacity compared with wireless backhaul links. There is a demand for ultra-high data rate backhaul point-to-point wireless links for 5G cellular networks, due to their fast, easy and cost effective installation compared to fiber optic networks. However for backhaul applications, the mm-wave antenna should be high gain and directive due to the challenges posed by propagation losses. For the mobile radio access part of the network, including macro and small cell base stations, which is the main focus of this thesis, the antennas need to be designed to be able to scan the beam or switch between beams or beamform while communicating with users, as shown in Fig. 1.3.

Traditionally, phased array antennas are used for applications such as space communications, electronic warfare and radar functions [7]. The need for a beam scanning ability for the 5G base stataion has drawn the attention to phased array antennas, designed for mm-wave frequency bands. The possible allocated spectrum for 5G is shown in Fig. 1.4 [8]. As shown, the mm-wave bands are allocated in 3-4 separate bands. Providing an individual antenna system for each of these bands may not be feasible or not optimal in term of cost, complexity and available physical space. Therefore, Ultra-Wideband (UWB) antenna arrays, covering multiple mm-wave frequency bands represent a versatile candidate for future 5G antenna systems. Also it needs to be mentioned, as we move to higher mm-wave frequency bands, all the passive and active components in the system becomes smaller, which introduces hardware challenges such as integration, packaging and manufacturing cost. Therefore, in addition to having wideband characteristics, antennas for mm-wave frequencies

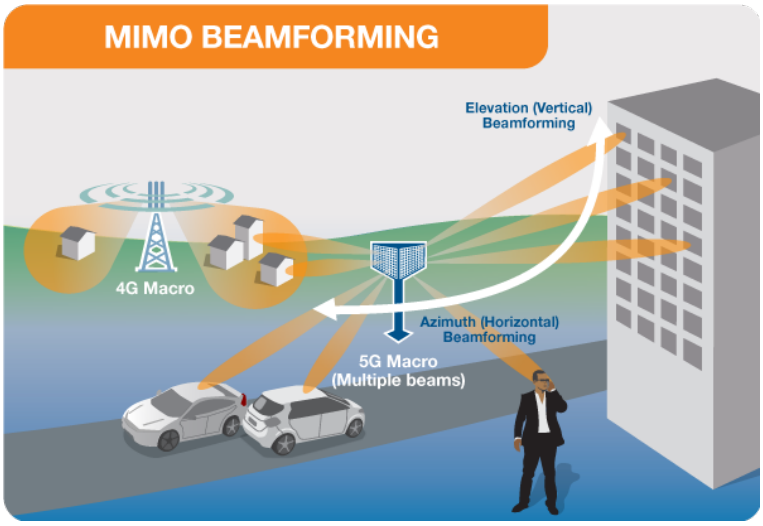

Figure 1.3: Comparison of a 5G base station with the ability of beamforming and a 4G base station with wide beam [6].

should offer an easy integrating capability and low fabrication cost.

1.2 System Evaluation

In the past few years, the performance evaluation of wireless devices has shifted from conducted measurements to more realistic Over-The-Air (OTA) tests. In conducted testing, coaxial cables are attached to a designated testing or measurement port on the device. On the other hand in OTA testing, the performance evaluation of wireless devices is performed without disconnecting the antennas from its system. Thus, no modification of the Device Under Test (DUT) is needed [9, 10].

OTA tests of Single-Input Single-Output (SISO) devices or antennas can be categorized in terms of total radiated power (TRP) and total isotropic sensitivity (TIS) [11]. However, these parameters are not sufficient for characterizing the performance of Multiple-Input Multiple-Output (MIMO) wireless devices or antennas. MIMO technology uses multiple antennas at both the transmitter and the receiver sides to increase channel capacity and the reliability of the communication system [12].

In MIMO OTA tests, the characteristics of the antenna and the propagation channel play key roles. As antennas are inherently included in OTA testing, it is important to also consider realistic channel models for MIMO device-performance evaluation. A realistic propagation channel model can vary for different applications. Thus, evaluating the OTA performance of devices in each possible propagation channel can be unrealistic, time consuming, complex and expensive. One way to simplify

Figure 1.4: Global snapshot of 5G spectrum [8].

the testing procedure is to evaluate the performance of the system in the extreme (or edge) propagation channels, and put some specific weights on the performance characterization parameters in theses extremes based on where the real propagation environment stands. In [13] two extreme reference environments, useful for OTA tests are defined: the Rich Isotropic Multipath (RIMP) which can be emulated in reverberation chambers and the Random-Line of Sight (Random-LoS) emulated by anechoic chambers. These two extreme reference environments are complementary and real life can be somewhere in between. The performance of the antenna can be then evaluated in these environments and depending on the results, modification of the design can be applied based on the relevance of either environment for the specific application. For example, hand-held wireless devices used in urban and indoor areas are mostly subjected to multipath propagation and hence, the RIMP can be dominant. On the opposite, the Random-LoS is more relevant for cars moving along highways communicating with base stations and other cars [14, 15]. Also, the LoS channel is likely to become more dominant as the carrier frequency of the transmitted signal goes higher.

Traditionally, antennas are characterized by their realized gain and radiation patterns [16]. However, antennas used in wireless devices such as cell phones and laptops are exposed to multipath, resulting in variation, or so called fading, of the received signal at the antenna. Therefore, antenna testing needs to take into account the signal variation which can be described by the cumulative distribution function (CDF). Moreover, multiple-port antennas can be used to mitigate the negative effects of fading with the help of antenna diversity and MIMO technology [12]. Making use of the statistical features of the received signals, different performance characterization parameters, or figures of merit, such as Diversity Gain (DG) [16] and MIMO multiplexing efficiency [17] can be defined. These are instrumental to evaluate the improvement achieved by using multiple antennas in a multipath environment. In a similar way, LoS performance evaluation should take into account the statistics of different users. A CDF can be used to describe the statistical variations of the received signal due to the randomness caused by arbitray locations of users and the way they hold their wireless devices [13, 18]. The performance evaluation in RIMP has been studied in many articles [19], while Random-LoS is a new, less conventional concept that is currently under development.

The ability to achieve a high port isolation, together with compact configuration, renders the dual-polarized antenna a promising option for MIMO applications, especially for micro-base station antennas when space is a limitation. The importance of dual-polarized antennas is emphasized since the maximum available independent channels in LoS are limited to only two, i.e., given by two orthogonal polarizations. Many different types of dual-polarized antennas has been suggested in the literature. However, the most challenging aspect is to comply with the wideband requirement while keeping the manufacturing cost and complexity as low as possible.

1.3 Aim of the Thesis

The thesis aims two individual but related research topics, as explained as follows.

1.3.1 OTA Evaluation and Design Modification Based on a New Characterization Method

MIMO OTA performance assessment of antenna systems in 3G and 4G wireless communications systems is highly relevant. Therefore, antennas designed for MIMO applications need to be characterized, optimized and tested based on their system performance in the relevant propagation environment. In order to address the above and to be able to relate the OTA throughput measurement to the traditional way of evaluating the antenna performance in terms of radiation pattern and gain, the received signal at the output ports of antennas can be interpreted as the probability of detection [20].

The received signal can be computed based on the embedded radiation pattern of the antenna and the model of the propagation environment. Having simplified the system performance analysis, the OTA performance of the system can be simulated. The design of the antenna can be readily readjusted and modified to meet the required system performance specifications. It is worthwhile to note that although, the classical evaluation of the antenna might not be completely sufficient, it gives us a good approximation to start our design, which can be subsequently modified based on the OTA simulations. Also, in order to verify the antenna design concept and its performance in the simplified environments, OTA measurements need to be performed to verify compliance with the specified requirements. In this thesis, a new characterization method is used to evaluate and modify the design of the self-grounded bowtie antenna for micro-base station application. Furthermore, the antenna hardware is devised to perform OTA measurements in an emulated Random-LoS environment.

1.3.2 Designing Wideband Wide-scanning Phased Array Antenna for mm-wave 5G Base Stations

The fifth generation (5G) of wireless communication will make use of several mm-wave frequency bands, varying from 20 to 70 GHz [21]. However, providing an individual antenna system for each of these bands may not be feasible nor optimal in term of cost, complexity and available physical space. Therefore, ultra-wideband (UWB) antenna arrays, covering multiple mm-wave frequency bands represent a versatile candidate for the future 5G antenna systems. In addition to having wideband characteristics, these antennas should offer an easy integrating capability with the active modules. There are several designs for UWB array antennas. Tapered-slot array antennas [22], tightly coupled dipole array (TCDA) [23], planar ultra-wideband modular arrays

(PUMAs) [24], Magneto-Electric Dipoles (MEDs) are some of the well-known designs for UWB arrays. However, as we move up to higher frequencies, all of the above mentioned arrays will face the scalability problem in terms of the manufacturing feasibility, fabrication cost and also the assembly complications. There are many antennas designed for mm-wave frequency bands including on-chip antennas [25] and Low temperature cofired ceramic (LTCC) multilayer antennas [26]. However, It needs to be mentioned that all these mm-wave antennas are relatively narrow band with an impedance bandwidth of less than 25%. In this thesis, we present some fully planar designs of UWB planar arrays with large beam scanning capabilities and bandwidth exceeding 65% for mm-wave base station applications. The antennas are realized using a simplified standard PCB manufacturing technique which provides a low fabrication cost.

1.4 Thesis Outline

This thesis is divided into two main parts. The first part has been organized in 4 chapters and introduces the background needed for better understanding the appended papers, presented in the second part. In the second part of the thesis, the author's most relevant contributions are included in the form of appended papers. Additional non-appended publications can be found as references in the section List of Publications.

In **Chapter 2**, a systematic approach to characterize the OTA performance of wireless devices in two extreme edge environments is presented and the appropriate figure of merits to evaluate the performance of MIMO systems are introduced. Also in this chapter, the Threshold receiver model is introduced as a model to relate the system throughput to the received power at the antenna ports. Further on, the reader is introduced to different types of wideband dual-polarized antennas for base station applications, together with different wideband balun structures. The self-grounded bowtie antenna is also introduced in this chapter, together with the array antenna specification for a MIMO OTA measurement set-up in Random-LoS. In **Chapter 3**, an introduction to phased array antenna as a promising candidate for beam-steering base stations is presented. Also, we try to explain the scan blindness phenomena in the array of dipoles, caused by the surface wave and the feed lines. Further on, tightly coupled dipole arrays (TCDAs) are introduced as an UWB wide beam-steering array with the ability to be integrated with the active circuitry. The concept of these arrays is explained based on the Wheeler's current sheet model and different examples from the literature are provided. Finally, **Chapter 4** concludes the first part with a brief summary of the included papers and future works.

Part II of the thesis includes the most relevant research papers. In Paper A, we improve the MIMO performance of a 2-port self-grounded bowtie antenna in Random-

LoS by using a system characterization based on a MIMO efficiency metric. We show that the polarization orthogonality and power imbalance are the two important factors which contributes to degrade the MIMO performance in a Random-LoS propagation environment. In Paper B, we design a wideband dual-polarized array antenna for OTA Random-LoS measurement set-up for automotive wireless systems, covering multiple LTE bands. Paper C presents two small array antenna structures comprised of bowtie elements to achieve an omni-directional coverage for MIMO applications. The elements are modified to have a desirable MIMO performance in RIMP and Random-LoS. This has been done by investigating the MIMO efficiency metric in the edge propagation environments. In Paper D, a fully planar UWB linearly-polarized design for mm-wave phased arrays is presented. The proposed antenna has a large beam steering ability and can be manufactured using standard PCB technology. Paper E provide us with another design for wideband wide scanning linearly polarized phased array element in an aperture coupled feed structure. A dual-polarized planar UWB element for phased arrays is proposed in Paper F.

Chapter 2

System Evaluation and OTA Considerations

OTA measurements allow us to test wireless devices in an emulated typical propagation environment. Having a reliable test setup requires an accurate and repeatable model for the propagation environment. To address this, various OTA methodologies have been proposed and discussed in the standardizations [27]. The methodologies vary in terms of propagation environments, system simplicity and cost. In general, the existing methods can be divided into two main categories: measurements in anechoic chambers and measurements in reverberation chambers. The anechoic chamber methods can be conceptually simple but it comes with low flexibility of the propagation channel model [10]. The more flexible methods performed within an anechoic chamber will result in higher complexity and therefore higher costs too. On the other hand, methods using reverberation chambers are much simpler and more cost-efficient, but may have difficulties to control the channel model. These types of difficulties can be overcome by adding RF absorbers, cascading two or more reverberation chambers and adding channel emulator to the downlink which increase the complexity and cost [10].

2.1 Edge Environments and the Hypothesis

In [13] two extreme reference environments, convenient for OTA tests are defined: the Rich Isotropic Multipath (RIMP) which can be emulated in reverberation chambers and the pure-LoS emulated in anechoic chambers. These two reference environments are complementary and real life propagation channels can be somewhere in between.

2.1.1 Rich Isotropic Multipath (RIMP)

In urban and indoor environments, wireless terminals are subject to strong fadings due to multipath propagation [28]. This happens because of the reflection, diffraction, scattering and refraction from objects in the environment such as the ground, buildings, trees and people. At the receiver side, the multipath environment can be characterized by several incoming plane waves. These incoming waves can have a certain angle of arrival (AoA) distribution. However, if there is no LoS and the number of incoming waves (richness) is large enough with statistically arbitrary arrival direction, then the received signal's amplitude and power become Rayleigh and exponentially distributed, respectively. Note that, a richer environment is needed for more directive antennas than the non-directive antennas. On the other hand, wireless terminals might have a preferred usage orientation in respect to a specific axis. Cross-polar Power Discrimination (XPD) [29] is defined to describe the polarization purity. However, we refer to this as polarization imbalance in the environment. The RIMP environment is a result of polarization balance and large enough uniform AoA distribution over the whole sphere. An illustration of the incoming waves in RIMP is shown in Fig. 2.1. Since the RIMP environment is characterized by uniformly distributed AoAs and balanced polarization, the evaluated performance of the wireless device becomes independent of its orientation. In such an environment, the radiation pattern plays a very minor role, if any role at all. This is due to the statistically fluctuated received signal caused by the constructive and destructive combination of incoming waves with arbitrary amplitude, phase, polarization and AoA [30].

The RIMP environment can be emulated in reverberation chambers. The reverberation chamber is a large metal cavity provided with mode stirrers and antennas. Traditionally, it is used for electromagnetic compatibility (EMC) measurements [28, 31]. This ability of emulating RIMP channels made the reverberation chamber a versatile tool for OTA testing. It has been shown that the reverberation chamber can provide accurate and cost effective OTA characterization of passive antennas in terms of the antenna efficiency, diversity gain and maximum available MIMO capacity [16,32–34]. It also can be used to characterize active devices in terms of total radiated power (TRP) and total receiver sensitivity (TIS) and throughput data rate [20,35]. In [36–39], the control of coherence bandwidth and Doppler spread inside the reverberation chamber has been studied. Also, it has been suggested in [10] that channel emulators can be employed to the downlink prior to the launch of the signal into the chamber to fully control the channel model. The tests performed in reverberation chambers are statistical in nature. Therefore, the signal variations due to fading, measured at the receiver antenna port can be described in terms of the cumulative distribution function (CDF).

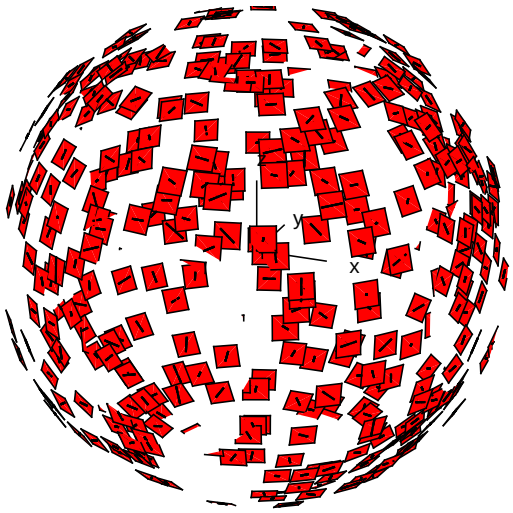

Figure 2.1: Illustration of the incoming waves in RIMP, with random AoA, polarization, amplitude and phase.

2.1.2 Random Line of Sight (Random-LoS)

Traditionally, all antennas have been characterized in terms of their far-field patterns and realized gains. Measurements have therefore been performed in anechoic chambers with a pure-LoS link between the transmitter and the receiver. However, this approach can only be valid for fixed antennas in point-to-point applications. The LoS in wireless communications can deviate from the traditional definition. Because of the arbitrary distribution of the users' locations, as well as the position and orientation of the devices they use, the LoS component between users and base-stations can be random. Arbitrary locations of users, results in randomness in terms of AoA, and the different orientations of the device causes the wireless devices to experience a Random-LoS in terms of polarization [13, 18, 30]. The randomness in LoS was previously studied in [40, 41], but the term Random-LoS in a 3D context, taking into account the user distribution to statistically evaluate the performance of antennas and wireless devices, was first presented in [30]. The illustration of Random-LoS in terms of AoA and polarization is shown in Fig. 2.2.

We can conclude that in a pure-LoS environment, testing of wireless devices and antennas should also be statistical, due to the randomness of a mobile users, both in location (AoA) and in orientation of the device (polarization). This statistical variation is present even for stationary users, within an ensemble of users. In this random-LoS propagation environment, the randomness can cause a slow fading determined by the radiation pattern of the antenna. Random-LoS, similar to Pure-LoS can be emulated in anechoic chambers. Some automotive active OTA measurement in Random-LoS have been performed and presented in [42, 43].

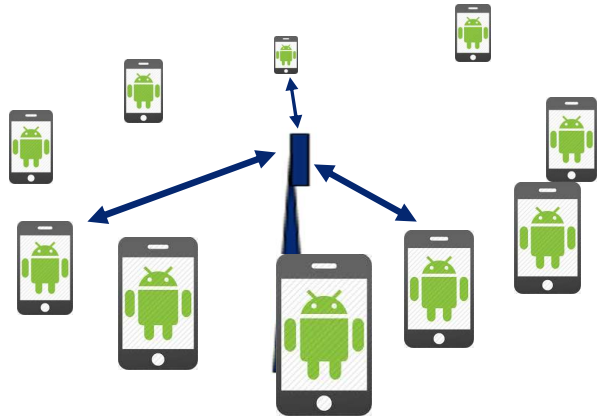

(a)

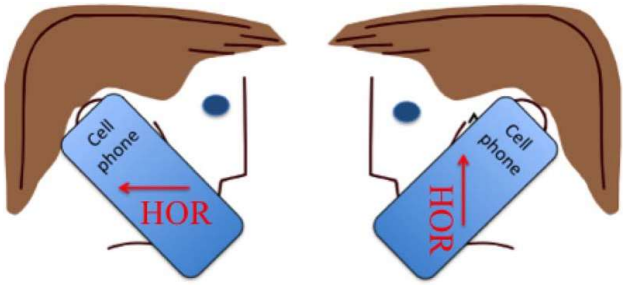

(b)

Figure 2.2: Illustration of the Randomness of LoS component in terms of a) AoA and b) Polarization [30] in Random-LoS.

2.1.3 Real life hypothesis

The aforementioned edge propagation environments are opposite and extreme environments which rarely represent the actual propagation environment. Real life propagation environments will always be somewhere between these two extremes. Based on this pre-assumption, a real life hypothesis has been stated in [13] as: "*If a wireless device is tested with good performance in both Random-LoS and RIMP environment, it will also perform well in real-life environments and situations, in a statistical sense.*" The importance of these edge environments has also been argued in [44, 45].

2.2 System Characterization

As mentioned above, antennas in RIMP and Random-LoS propagation environments can be characterized statistically and the signal variation on the receiver ports can be described by a cumulative distribution function (CDF). This signal variation can be seen as the fluctuation of the signal received by a moving user or a group of stationary users. Multiple-port antennas can be used to mitigate the negative effects of these variations in the form of antenna diversity and multiple-input multiple-output technology.

2.2.1 Diversity

Using multiple antennas at the receiver side to detect multiple copies of the same transmitted signal and combine them in a proper way can result in an improvement of the received signal level. The reason behind this can be discussed differently in two different environments. In a multipath propagation environment, signals received at the antenna ports are the result of constructive and destructive combinations of signals passing through different paths, therefore different ports may experience different fading. If the received signals at the receiver ports are uncorrelated, the transmitted signal can be extracted at the receiver side more accurately by using different combinations of the received signals. This is due to the fact that since signals at the receiver ports are uncorrelated, it is very unlikely they would experience a fading dip in all the received signals, simultaneously [16]. This is known as diversity combining and can be implemented in different ways. Frequency, spatial, pattern and polarization diversity are different types of diversity. In Random-LoS, there is no signal fluctuation due to destructive and constructive combination of multiple received components. However, the one incoming wave (LoS component) can arrive from a random AoA and with a random polarization resulting in fading related to the farfiled functions of the receiver antennas. Since having spatial diversity in LoS is impractical and needs a large separation between ports [46], polarization and pattern diversity are promising options in this type of propagation environment. To combine the received signal at different ports, there are several schemes that can be used, such as Selection Combining (SC), Equal Gain Combining (EGC) and Maximal Ratio Combining (MRC) [12]. In MRC, the output of the combiner is the weighted sum of received signal at each port that maximizes the receive power or, more generally, the SNR. These weights are the complex conjugate of the received voltage at each port.

By plotting the CDF of the combined received signal, the diversity gain (DG) can be defined as the power or SNR improvement achieved by a diversity antenna system as compared to a single reference antenna, usually at the 1% CDF level. In Random-LoS this is the increase in the received power of the 1% worst users or cases during a fading, when the transmit power remains the same. In RIMP, it is the increase in the received power of the 1% worst signal levels, when the transmit power remains the

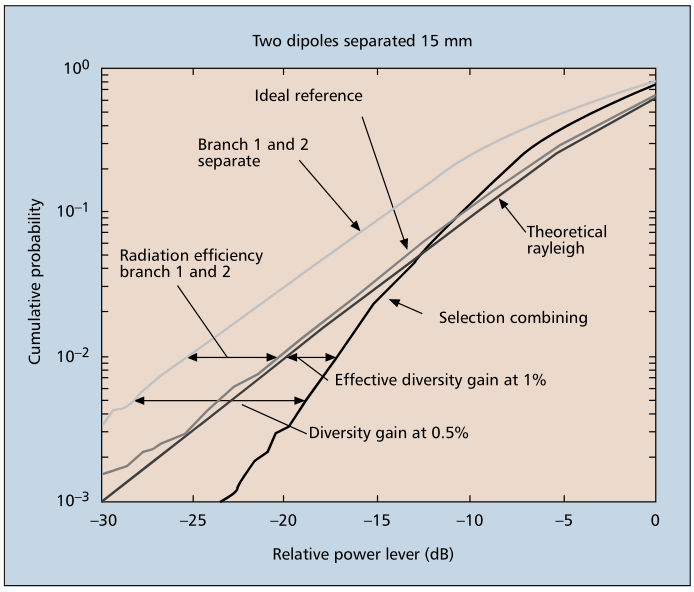

Figure 2.3: The cumulative probability distribution function (CDF) of measured S_{12} in reverberation chamber for two paralell dipoles diversity antenna and an ideal reference [16].

same. We can distinguish between apparent, effective and actual diversity gains [47] depending on whether the reference antenna is one of the diversity branches, an ideal antenna with 100% total radiation efficiency or an existing practical reference antenna. Since the CDF of the envelope of the voltage induced at a single port antenna follows the theoretical Rayleigh distribution, the descriptive unit dBR is introduced to quantify the diversity gain in RIMP [47]. In Fig. 2.3, the CDF of the normalized transmission (S_{12}), measured in the reverberation chamber is shown. We can see that for the ideal reference, the curve follows the theoretical Rayleigh distribution, while for each parallel dipole the curves are still similar to the theoretical Rayleigh but shifted to the left, because of lower radiation efficiency. After applying the selection combining algorithm, we can define the effective diversity gain as the difference between the selection combined CDF and the theoretical Rayleigh curve at the 1% level. However, using this unit in Random-LoS might not be very representative, since the CDF of each antenna follows the farfield function and not the Rayleigh distribution. Although studies in [48] have shown that they can be similar if the antenna is not directive and surrounded by scattering bodies such as the chassis of the device and the user's head and hand.

2.2.2 Threshold Receiver Model

The threshold receiver model is a model for calculating the throughput data rate of a practical wireless device, based on the CDF of the output power at the antenna port [20]. The relative throughput obtained in this way can be further interpreted as the probability of detection. The model can be explained as follows.

In a static additive white Gaussian noise (AWGN) channel, the Group Error Rate (GER) can change very abruptly from almost 100% to 0% at a certain threshold, if the forward error corrections (FECs) is used:

$$\mathrm{GER}_{IDEAL}(P) = \begin{cases} 1 & P < P_{th} \\ 0 & P > P_{th} \end{cases} , \tag{2.1}$$

where P is the received signal power and P_{th} is the threshold. Then the throughput data rate can be expressed by:

$$\mathrm{Tput} = \mathrm{Tput}_{max} * \{1 - \mathrm{GER}(P)\} , \tag{2.2}$$

where $\mathrm{Tput}_{\mathrm{max}}$ is the date rate determined by the wireless system specification. This formula is valid for the GER in a stationary LoS channel versus a constant signal power P and for the GER averaged over long enough fading time, verus average signal power in a dynamic fading environment. These two are related to each other as

$$\mathrm{GER}_{av}(P_{av}) = \int_0^\infty \mathrm{GER}_{LOS}(P)\mathrm{PDF}(P/P_{av})dP , \tag{2.3}$$

which gives

$$\mathrm{Tput} = \mathrm{Tput}_{max} * \mathrm{CCDF}(P_{th}/P_{av}) . \tag{2.4}$$

We can conclude that in a dynamic channel, the relative throughput is directly related to the complimentary cumulative distribution function (CCDF) of the power distribution at the threshold. According to [49], in a fading environment, if the instantaneously received power is above the threshold, we will detect the channel with no errors, otherwise we will not detect it. Therefore, we can find the average throughput by counting the number of times the received power is above the threshold during the fading cycle, i.e., the number of detections of the channel. Thus, the relative throughput becomes equal to the probability of detection (PoD).

$$\mathrm{PoD}(P/P_{th}) = \frac{\mathrm{Tput}(P/P_{th})}{\mathrm{Tput}_{max}} = \mathrm{CCDF}(P_{th}/P) , \tag{2.5}$$

where P is the reference power proportional to transmitted power, P_{th} is the dynamic threshold level and CCDF is the complimentary cumulative distribution function of the received fading power, normalized to the reference.

Although the ideal threshold receiver model was first introduced for modeling the throughput in RIMP, it has been expanded to Random-LoS, because of the statistical behavior of signal introduced by the randomness in this propagation environment [43]. Note that, in RIMP, the average signal power of a Rayleigh distribution can be used as the reference power, while for Random-LoS, it can be chosen based on the application. For example, the reference power can be the maximum received power of the actual scenario [50], or the received power of an ideal antenna [51, 52].

2.2.3 MIMO

Systems with multiple antennas at the transmitter and the receiver sides are commonly referred to as Multiple-Input Multiple-Output (MIMO) systems. These multiple antennas can be used to increase the date rate and improve the performance through multiplexing and diversity [12]. In multiplexing, independent data can be sent through independent paths and will then be separated at the receiver sides. Assuming a narrow band MIMO channel (or flat channel for each OFDM, i.e., orthogonal frequency division multiplexing, subcarriers), the input-output relationship in communication systems can be represented as

$$\mathbf{y} = \mathbf{H}\mathbf{x} + \mathbf{n} \ , \tag{2.6}$$

where $\mathbf{H}$ is the MIMO channel, $\mathbf{x}$ and $\mathbf{y}$ are the transmitted and received signal vectors, respectively, and $\mathbf{n}$ is the noise vector with independent and identically distributed (i.i.d) unite variance Gaussian elements [17].

Depending on the availability of the channel state information (CSI), we can use different ways to separate data bitstreams at the receiver side. If the CSI is known at both the transmitter and the receiver side, singular value decomposition (SVD) can be used to differentiate data streams [53]. However, due to finite coherence time of the fading channel, and the use of different frequencies in the up- and down-link, the CSI is usually unknown at the transmitter side. Another method to extract data without the need of knowing the channel at the transmitter side is to use the Zero-Forcing (ZF) receiver, which relies on the pseudo-inverse of the channel matrix at the receiver side. Following [53], the SNR of the i_{th} stream using a ZF receiver can be obtained by

$$\gamma_i^{ZF} = \frac{\gamma_t}{N_t[(\mathbf{H}^H\mathbf{H})^{-1}]_{i,i}} \ , \tag{2.7}$$

where γ_t is the transmit SNR, $[\mathbf{X}]_{i,i}$ denotes the i_{th} diagonal element of the matrix $\mathbf{X}$, $\mathbf{X}^{-1}$ and $\mathbf{X}^H$ are the inverse matrix and the conjugate or Hermitian transpose of the matrix $\mathbf{X}$, respectively.

The ideal threshold receiver model can be used to plot the PoD curve for multiple data streams based on the CDF of the received power. The PoD of the theoretical

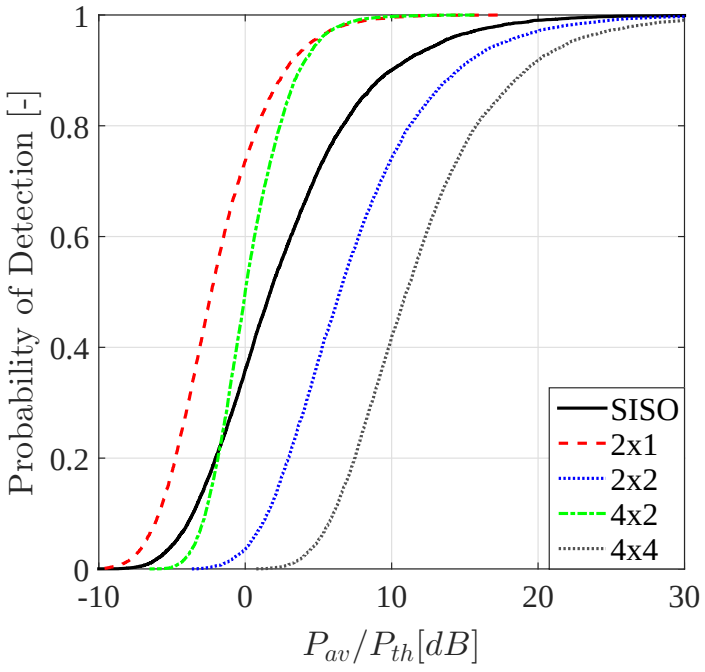

Figure 2.4: The PoD of different order MIMO systems for i.i.d. received channels in RIMP.

i.i.d. (independent and identically distributed) Rayleigh channel with up to 4 bitstreams in a 4x4 MIMO system has been illustrated in [18]. Using ZF receiver, the PoD of detecting all bitstreams will be equal to the PoD of detecting the weakest channel for each realization of the channel. Also we need to mention that in RIMP, it is possible to have multiple i.i.d. channels. However, in Random-LoS, we can not get more than two data streams corresponding to the two orthogonal polarizations, unless we separate the antennas by a very large distance or use spatially separated very high gain antennas [17].

As an example, the PoD of 1, 2 and 4 bitstreams for different order MIMO systems, using threshold receiver model and ZF receiver are shown in Fig. 2.4. We assume i.i.d. ports in a RIMP propagation environment. By comparing the higher order MIMO with SISO case at 95% PoD level, we can see that, for example, 4.8 dB more power compare with SISO is needed to detect 95% of the cases in 2x2 MIMO. This power cost for 2x1, 4x2 and 4x4 MIMO systems are -8.9 dB, -8 dB and 9.2 dB, respectively.

MIMO Efficiency

The MIMO efficiency has been introduced in [17, 54] in order to define a figure of merit to evaluate the MIMO system performance. To compute the MIMO efficiency, we need to plot the PoD of single or multiple bitstreams using the Threshold receiver model. As known, the diversity gain is often defined at the 1% CDF level [47, 55]. However, to verify this value in a practical situation, we need a large number of samples. Instead we can investigate the diversity gain at the 5% CDF level. Following this, we can find the MIMO efficiency by comparing the value of P/P_{th} at the 95% PoD level to an ideal reference case.

$$\eta_{\text{MIMO}} = \frac{\text{PoD}_{\text{ref}}^{-1}(0.95)}{\text{PoD}^{-1}(0.95)}, \tag{2.8}$$

where PoD^{-1} is the inverse function of PoD^{-1} and $\text{PoD}_{\text{ref}}^{-1}$ is the inverse function of the probability of detection of the reference case. The degradation of the actual scenario compared to the reference, implies the higher transmit power needed to detect 95% of cases compared to the ideal antenna. Note that to have a fair comparison, coding and modulation methods remains the same for both cases. The 95% PoD level corresponds to the 95% relative throughput level.

The ideal reference can be different in RIMP and Random-LoS case. In RIMP, we can use antennas with 100% efficiency and no correlation, with the same order of MIMO, as the reference, resulting in independent and identically distributed (i.i.d.) voltage signals. The practical antennas will always have lower performance than the reference in a RIMP propagation channel. In Random-LoS, the i.i.d. case do not represent a theoretical limit [17]. The statistical characteristics in Random-LoS is due to the randomness of the AoA and polarization of the LoS component directly related to the farfield function of the antenna. So in this environment, the limit cannot be defined by the i.i.d. channel, instead by specific conditions for the farfiled function of an ideal antenna [51, 52]. So in Random-LoS, the reference is defined as a 1- or 2-port (maximum bitstream which can be achieved in LoS) antenna with 100% total radiation efficiency and matched coverage and polarization. Matched coverage means that the radiation pattern of the reference antenna should cover the intended angular coverage with a uniform realized gain and matched polarization means that the receiver antenna should be able to detect all the power delivered by the incoming wave with random polarization. In the 2-bitstream case, it means that the radiation function of two receiving ports should remain orthogonal for the whole desired coverage. Note that in Random-LoS, the number of the actual receivers can be defined in such a way to be larger than the number of the ports in the ideal reference. In this case, the MRC diversity gain achieved by using a larger number of ports might result in having a MIMO efficiency larger than 0 dB.

2.3 MIMO Hardware

2.3.1 Wideband Dual-Polarized Antennas for Base-Stations

As discussed above, MIMO antennas can provide diversity gain, multiplexing and increase the channel capacity. Making use of ports with high isolations can help us to achieve higher order of MIMO in the RIMP propagation environment, even in a small area. For the case of LoS (or Random-LoS), the maximum number of independent subchannels are restricted to two orthogonal polarizations. This put more importance on the use of polarization-MIMO where two orthogonal polarizations are used as MIMO subchannels. Using polarization diversity and multiplexing can also lead to more compact structures. This is especially important for wideband micro-BTS applications [56, 57].

Through the years, many different types of wideband dual-polarized antennas have been proposed for base-station applications. Multilayer aperture-coupled patch antennas were studied in [58–60]. In these antennas, two orthogonal apertures (usually H-shaped slots) excite one single patch in two orthogonal polarizations. Dual-polarization can also be achieved by using L-shaped probes [61, 62]. In [63] it has been shown that using L-shaped probes can increase the bandwidth. Several broadband cross-dipoles also have been presented in [64–67]. However, the multilayer stacked patch antennas are quite challenging in terms of manufacturing aspects. The proposed antenna in [65] consists of two orthogonal dipoles, a metal reflector and a dielectric post to support the cross-dipole on top of the reflector. The coaxial cables pass through the post and feed dipoles. To achieve this type of feeding, a wire bridge, i.e., copper connector is needed for each dipole. Therefore the feeding structure in this method needs to be arranged correctly in order to avoid intersecting. Another structure of cross-dipoles has been introduced in [66] which adds two short pins to improve the isolation between the ports. In [67] a double sided PCB printing approach has been used to improve the manufacturing complexity. Another design for wideband dual-polarized antenna can be achieved by the Magneto-Electric Dipole (MED) [68–70]. This is a complimentary antenna consisting of two cross electric dipoles connected to vertically oriented shorted patch antennas. T-shaped probes are used as feeds where each probe has three parts. The first part which is vertically oriented, together with a vertical plate, works as a microstrip line on an air substrate. The horizontal part of the probe excite the electric dipole and the shorted patch, simultaneously. The last vertical part of the feed together with the other vertical plate, works as an open-circuited microstip line. Because of the air gap between different parts in this method, the structure might not be very stable and some supports need to be added. Taperd slot antennas are another ultra wideband dual-polarized antenna [71, 72]. However, they might be treated as high profile structures. Also, dual-polarized antennas might not have an integrated feeding structure or have separate feeding network, or both [73]. Different methods to

achieve widenband dual-polarized antennas are showed in Fig. 2.5

2.3.2 Balun

Baluns can be used to convert balanced to unbalance signals and vice versa. Many different balun structures have been reported in literature. Microstrip to coplanar stripline (CPS) and microstrip to parallel stripline transition are presented in [74] and [75] respectively. They are usually large in size and not suitable for compact structures. A broadband SIW planar balun is proposed in [76]. However, the size is still large for the application we consider in this thesis. Marchand baluns are another ultra wideband solutions. There are many different configurations of Marchand baluns, which makes them a popular approach for wideband applications [77–79]. In [73,80] a single layer octave bandwidth balun was introduced consisting of a Wilkinson power divider and a non-coupled line broadband phase shifter. Also the Composite Right Left Handed (CRLH) Transmission Line (TL) which exploits the phase advance of the left handed materials is another option to achieve wideband characteristics in a compact space [81]. In order to cover a 2:1 bandwidth while maintaining a compact size to have the ability to integrate 2 baluns with a dual-polarized antenna, artificial right/left handed transmission lines are used. Fig. 2.6 shows some examples of the mentioned baluns.

2.3.3 Self-Grounded Bowtie Antenna

The self-grounded bowtie was first introduced in [82]. It consists of a bowtie dipole above a ground plane. The bowtie structure gives the antenna the frequency independent characteristics and the ground plane helps the antenna to achieve a directional radiation pattern. To make the antenna more compact, the structure is then truncated and the outer end is connected to the ground plane. A 4-port dual-polarized structure of the self-grounded bowtie is proposed in [83]. In that study, the profile of each of the petals has been modified to achieve a good performance in the two modes of operations, i.e., the 4-port mode where each port is excited individually and the 2-port mode where 2 opposite ports are excited differentially. However, the overall structure of the antenna was relatively complex to manufacture.

2.3.4 Wideband Dual-Polarized Linear Array for MIMO OTA Testing in Random-LoS

Autonomous cars will most likely play a major role in transportation systems in the near future. To achieve their potentials such as route planning, human safety, fuel efficiency, etc., autonomous cars should have a fast and reliable connection to the nearby networks and to other cars. Therefore, OTA (Over-The-Air) performance testing of wireless communication to cars will become critical. Among the two above

mentioned edge or extreme models for propagation environment, the Random-LoS will mostly dominate for automotive car applications, as cars are mostly on the roads and highways. The pre-dominance of the Random-LoS will be emphasized as the frequency increases, i.e., in millimeter wave applications. To address this, the preliminary Random-LoS measurement set-up was presented in [14]. In that setup, a car was located on a turntable in an anechoic or semi-anechoic chamber. In the initial measurements of an active LTE MIMO (shark-fin) car-mounted antenna in Random-LoS, a single bowtie element antenna was used as the chamber antenna [42].

However, a much larger antenna may be needed to obtain a large enough test zone emulating an incident plane wave at the DUT. A preliminary study for an array configuration for this measurement set-up has been done in [15]. In [84] a cylindrical reflector in conjunction with a linear array has been used as the chamber antenna for OTA test of automotive wireless systems in anechoic chambers. This structure models base station antenna's height and tilting. In the analysis, the elements of the linear array were modeled with Huygens sources. An illustration of the concept is shown in Fig. 2.8. To fulfill the requirements for the array in a more realistic way, an array element with similar characteristics as the Huygens source must be designed. Besides being dual-polarized, the bandwidth of the element should cover various LTE bands (1.6-2.7GHz). The element spacing should be less than the free-space wavelength corresponding to the highest frequency, to avoid grating lobes. The actual element should have fairly constant beamwidth in the entire band of interest. Also, the final optimized antenna design should make the manufacturing cost as low as possible.

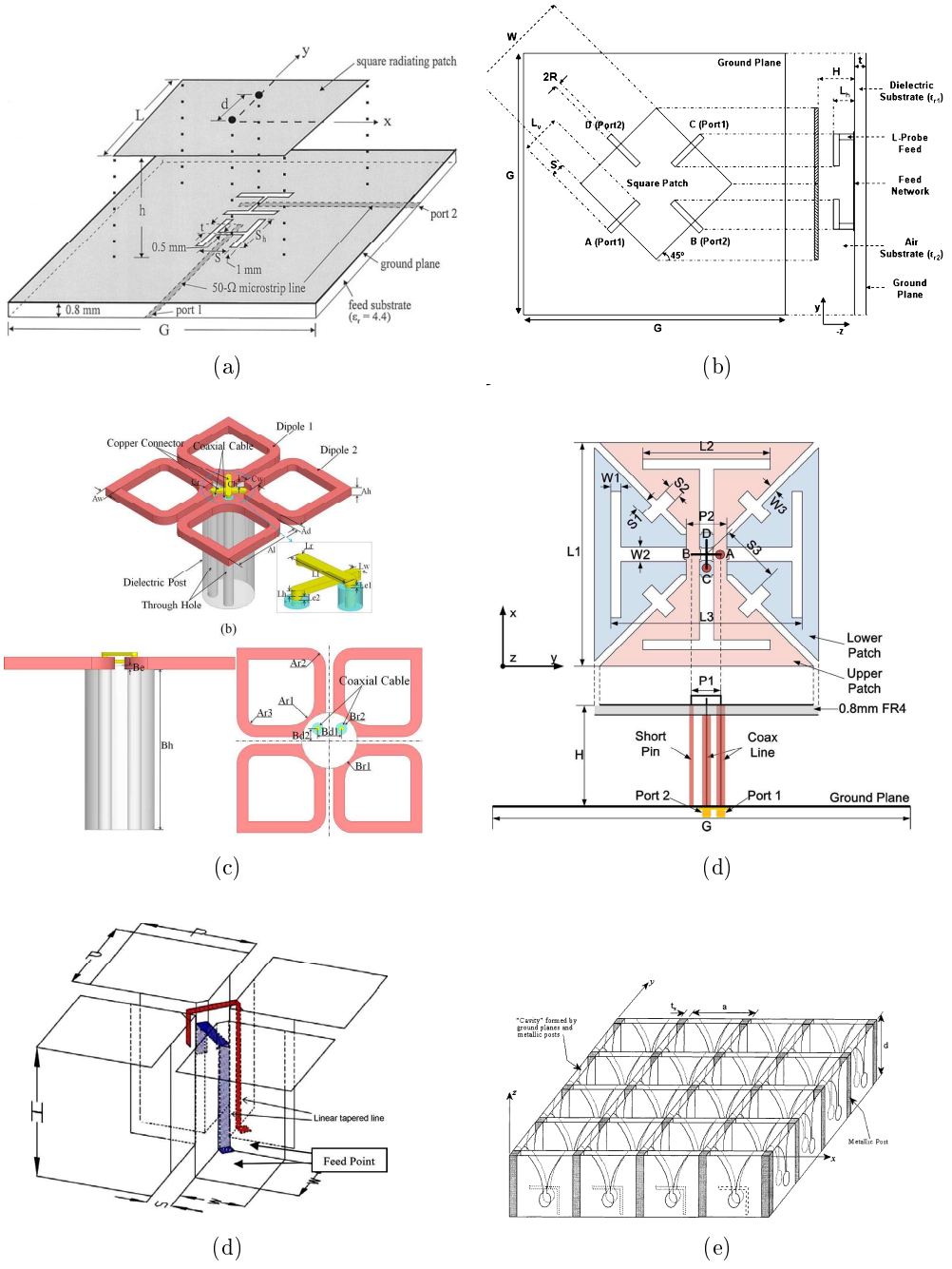

(a) (b) (c) (d) (d) (e)

Figure 2.5: Different aproaches for wideband dual-polarized antennas a) broad-band dual-polarized aperture-coupled patch [59], b) dual-polarized L-probe patch antenna [73], c) dual-polarized crossed-dipole antenna [65], d) coax-feed dual-polarized patch antenna consists of two pairs of T-shaped slots on the two bowtie-shaped patches [66], e) dual-polarized Magneto-Electric Dipole antenna [70], f) wideband widescan dual-polarized Tapered Slot antenna array [71]

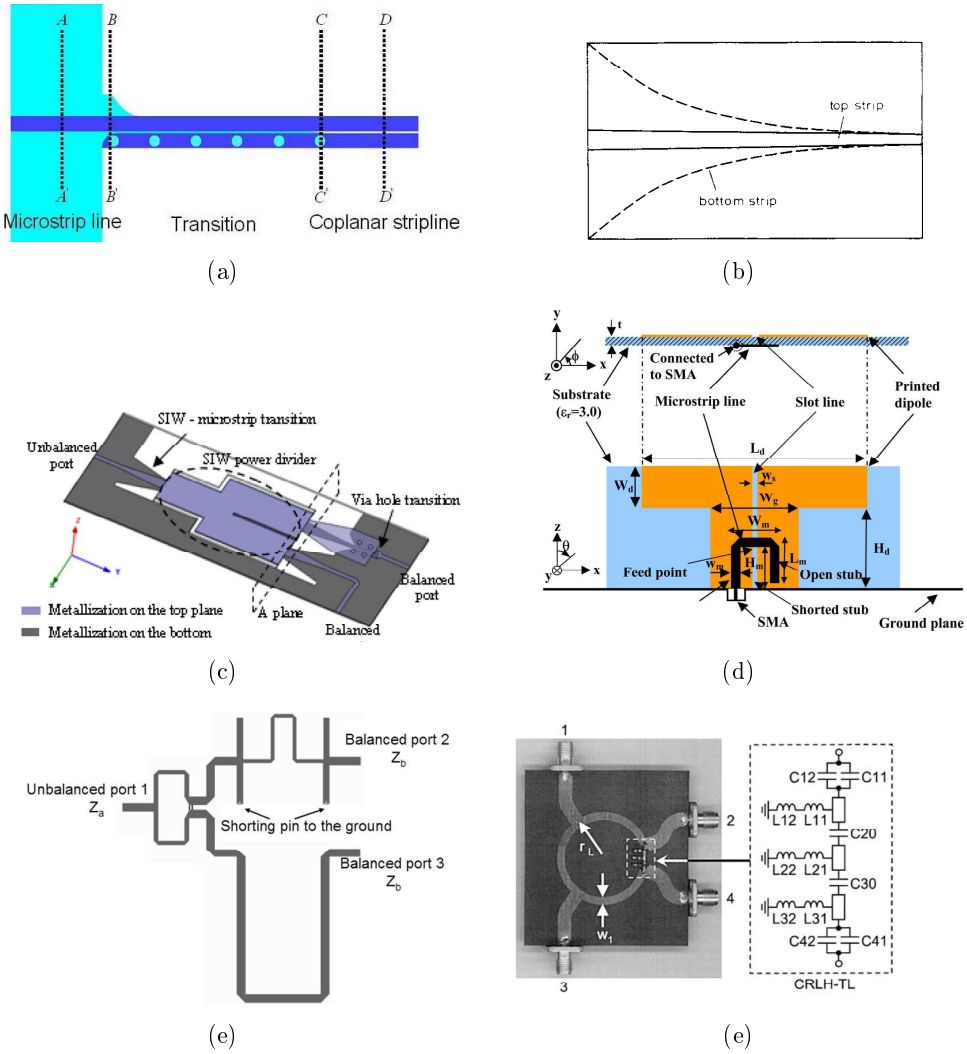

Figure 2.6: Different implementations of baluns a) microstrip-to-CPS [74], b) Microstrip-balanced stripline tapered transition [75], c) Substrate Integrated Waveguide (SIW) planar balun [76], d) Integrated Marchand balun with printed dipole [77], e) planar balun consists of a wide-band Wilkinson power divider and a noncoupled-line broad-band phase shifter [80], f) hybrid ring using an artificial lumped-element left-handed transmission-line [81]

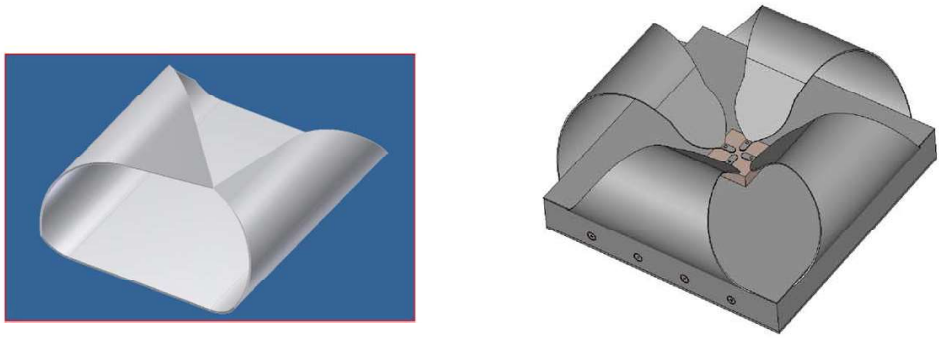

(a) (b)

Figure 2.7: Self-grounded Bowtie Antenna a) single-polarized version [82], b) dual-polarized version [83].

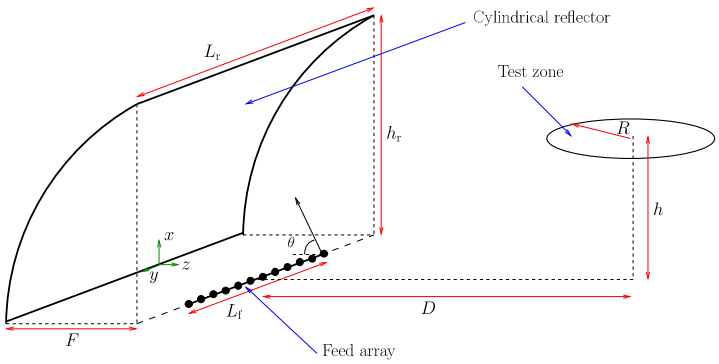

Figure 2.8: Illustration of a compact OTA measurement set-up for Random-LoS, consisting of a cylindrical reflector, linear array and the test zone [84].

Chapter 3

System Implementation for Beam-Steering Base Stations

One of the foreseen requirements for the 5G base station is to provide beam-steering, multiple-beams and beam-forming capabilities. Phased array antennas with the ability to change the shape of the beam electronically, introduce themselves as a versatile candidate for such applications. Among them, the designs in which the active circuitry can be monolithically integrated to the antenna elements has drawn much attention. Furthermore, due to the assignation of multiple bands at mm-wave frequencies to 5G applications, UWB arrays with the capability to cover multiple frequency bands can represent a beneficial solution. There are several technologies for UWB array antennas. Tapered-slot (often referred to as Vivaldi) array antennas are one of the most well-known designs for UWB arrays. It has been shown in [22] that Vivaldi arrays can provide a bandwidth of 10:1 at wide scan angles. However, their complex feeding mechanism together with their high-profile and complicated structure will make them expensive to manufacture and almost impossible to implement and assemble with reasonable cost. The tightly coupled dipole array (TCDA) has lower profile and can provide a large bandwidth of 9:1. The presence of the ground plane in these arrays, can isolate the radiating elements from the effects caused by the feed network. The substrate in these structures can be extended behind the ground plane for the integration of active circuitry, such as amplifiers, phase shifters, etc.

3.1 Theoretical Array Background

It is known that the antennas with large directivity should have a large aperture size in terms of wavelength. Traditionally, high gain antennas can be realized by reflector antennas. However, antenna arrays can be designed in a compact structure with the ability to shape and change the direction of the beam, by changing the amplitude and the phase of each element, electronically. The inter-element spacing

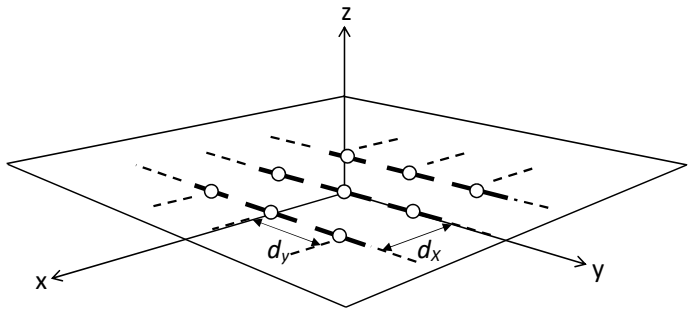

Figure 3.1: Geometry of the equispaced planar array. The center of the array is assumed to be at the center of the coordination system, i.e., $r_c = (0, 0)$.

can be considered as another degree of freedom for optimizing the arrays in terms of radiation pattern in so-called aperiodic arrays [85]. Despite these advantages, the antenna array solutions are normally more complex to design and expensive to manufacture compare to reflector antennas. The array antennas can normally have narrower bandwidth compared to reflector antennas. Arrays can be linear, planar or conformal and can be designed for full scanning, i.e., $\pm 60^\circ$ or more, or limited scanning. The elements of an array can be of many types, such as dipoles, slots, microstrip patches, horns and etc.

Let us assume M×N equispaced and identical antenna elements in xy-plane with their individual phase reference at

$$\mathrm{r}_{mn} = \mathrm{r}_c + (m - \frac{M+1}{2})d_x\hat{\boldsymbol{x}} + (n - \frac{N+1}{2})d_y\hat{\boldsymbol{y}}, \tag{3.1}$$

for $m = 1, 2, ..., M$ and $n = 1, 2, ..., N$, where r_c is the geometrical center of the array, d_x and d_y are the element spacing in $\hat{\boldsymbol{x}}$ and $\hat{\boldsymbol{y}}$ direction, respectively [28].

By using the superposition, the farfield function of the M×N planar equispaced array becomes

$$\boldsymbol{G}_A(\hat{\boldsymbol{r}}) = \sum_{m=1}^{M}\sum_{n=1}^{N} A_{mn}e^{j\Phi_{mn}}\boldsymbol{G}(\hat{\boldsymbol{r}})e^{jk\mathrm{r}_{mn}.\hat{\boldsymbol{r}}}, \tag{3.2}$$

where $\boldsymbol{G}(\hat{\boldsymbol{r}})$ is the embedded element far field function, A_{mn} and Φ_{mn} are the amplitude and the phase of the (m, n) element excitation, respectively. To simplify the design and analysis of the array, we can assume that all the elements in the array have the same element pattern. Therefore, the farfield function of the array can be written as

$$\boldsymbol{G_A}(\hat{\boldsymbol{r}}) = \boldsymbol{G}(\hat{\boldsymbol{r}})\boldsymbol{AF}(\hat{\boldsymbol{r}}), \tag{3.3}$$

$$\boldsymbol{AF}(\hat{\boldsymbol{r}}) = \sum_{m=1}^{M}\sum_{n=1}^{N} A_{mn} e^{j\Phi_{mn}} e^{jk\mathrm{r}_{mn}.\hat{\boldsymbol{r}}} \tag{3.4}$$

where $\boldsymbol{AF}(\hat{\boldsymbol{r}})$ is the array factor. The envelope of the array pattern is defined by the embedded element pattern while $\boldsymbol{AF}$ can be used to synthesize the array pattern. It needs to be mentioned that not all the elements in the array share the same embedded pattern due the mutual coupling e.g., the elements on the edges. The assumption that all the elements have the same embedded pattern becomes more accurate if the array is sufficiently large.

In order to scan the beam at the angle of (θ_s, ϕ_s) in so-called phased arrays, the excitation currents (or voltages) of the $(m,n)^{th}$ element should be phased as

$$\Phi_{mn} = -k\mathrm{r}_{mn}.\hat{\boldsymbol{r}}_{\boldsymbol{s}} = -k(\mathrm{x}_{mn}\boldsymbol{u} + \mathrm{y}_{mn}\boldsymbol{v}), \tag{3.5}$$

where $\boldsymbol{u} = \sin(\theta_s)\cos(\phi_s)$ and $\boldsymbol{v} = \sin(\theta_s)\sin(\phi_s)$ are referred to $u-v$ space. $x_{mn} = md_x$ and $y_{mn} = nd_y$ are the position of the $(m,n)^{th}$ element in respect to the center of the array. In terms of directivity, when planar arrays are used to steer the beam at the angle of θ_s, the directivity decreases with the factor of $\cos(\theta_s)$ in respect to the broadside radiation. This is due to the projection of the effective aperture into the observation direction [28].

The phased array antenna will introduce an unusual design challenge. That is the variation of the element impedance, not only for different frequencies, but also for each scan angle, due to the mutual coupling between the elements. A wide scanning angle can introduce a significant variation in the impedance which should be taken into account while designing the phased arrays. There are various designs which can provide a wide impedance bandwidth with wide scanning capabilities.

3.2 Scan Blindness

The scan blindness refers to the appearance of a single or multiple blind spots at some specific scanning angles in phased arrays, in which the reflection coefficient is one or close to unity. Although a true scan blindness (unit reflection coefficient) can only happen in infinite arrays, it can result in a sever impedance mismatch or a dip in active (embedded) element pattern for finite arrays, where the infinite array is blind [86].

3.2.1 Surface Wave Scan Blindness

This phenomena has first been studied in relation to waveguide arrays and its mechanism has been explained as a forced surface wave [87] or as a leaky wave [88] resonant response of the slow wave structure by phased arrays. This will also occur in

dipole arrays, since the grounded dielectric slab also supports a slow (surface) wave, specially when using thicker substrates for mm-wave applications. Using the same approach as in [86], here we try to investigate the scan blindness presented in printed dipole phased arrays. The approach can then further be expanded to other types of elements.

The farfield function of a x-directed dipole array on a dielectric slab for scanning to (θ, ϕ) can be formulated as

$$\boldsymbol{G}(x,y) = \frac{-jZ_0}{k_0 ab} \sum_{m=-\infty}^{\infty} \sum_{n=-\infty}^{\infty} \boldsymbol{Q}(k_x, k_y) e^{jk_x(x-x_0)} e^{jk_y(y-y_0)}, \tag{3.6}$$

where k_x and k_y are

$$k_x = (\frac{2\pi m}{a} + k_0 \boldsymbol{u}) \qquad ; \qquad k_y = (\frac{2\pi n}{b} + k_0 \boldsymbol{v}) \tag{3.7}$$

and

$$\boldsymbol{Q}(k_x, k_y) = \frac{(\epsilon_r k_0^2 - k_x^2) k_2 \cos k_1 d + j k_1 (k_0^2 - k_x^2) \sin k_1 d}{T_e T_m} . \sin k_1 d, \tag{3.8}$$

where

$$\begin{aligned}
T_e &= k_1 \cos k_1 d + j k_2 \sin k_1 d, \\
T_m &= \epsilon_r k_2 \cos k_1 d + j k_1 \sin k_1 d, \\
k_1^2 &= \epsilon_r k_0^2 - \beta^2, \\
k_2^2 &= k_0^2 - \beta^2, \\
\beta^2 &= k_x^2 + k_y^2, \\
k_0 &= \omega \sqrt{\mu_0 \epsilon_0} = 2\pi/\lambda, \\
Z_0 &= \sqrt{\mu_0/\epsilon_0},
\end{aligned} \tag{3.9}$$

where a and b are the element spacing in $\hat{\boldsymbol{x}}$ and $\hat{\boldsymbol{y}}$ direction, respectively. (x_0, y_0) is the center of the $(m,n)^{th}$ dipole, where $x_0 = ma$ and $y_0 = nb$ and $-\infty < m, n < \infty$. d is the thickness and ϵ_r is the relative permittivity of the dielectric slab.

For the arrays of dipoles, the scan blindness happens when the wavenumber β coincides with the propagation constant of a surface wave β_{sw} on the structure. Although the loading effect of the dipole should be included in determining β_{sw}, the transverse electric (TE) and transverse magnetic (TM) surface waves of the grounded dielectric slab can provide a fair approximation of β_{sw} to estimate the location of scan blindness. In general terms, the scan blindness occurs when the following three conditions are satisfied. (1) $\beta = \beta_{sw}$. (2) The element spacings (a and b) are such that $\beta = \beta_{sw}$ occurs for the values of $\boldsymbol{u}$ and $\boldsymbol{v}$ in real space. (3) The TM(TE) surface wave, due to $\beta = \beta_{sw}$, is not canceled by the zero value of $k_x(k_y)$, i.e., the polarization cancellation.

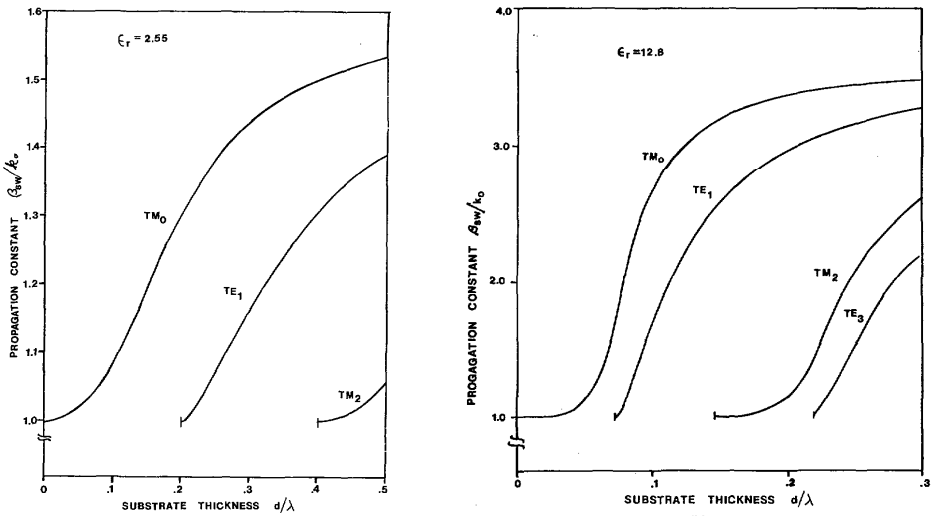

(a) (b)

Figure 3.2: Normalized surface wave propagation constants for grounded dielectric susbtrate with a) $\epsilon_r = 2.55$ and b) $\epsilon_r = 12.8$ [86].

As an example in [86], Fig. 3.2 shows the first few normalized surface wave propagation constants of the grounded dielectric, versus thickness for $\epsilon_r = 2.55$ and $\epsilon_r = 12.8$. As can be seen, increasing ϵ_r, as well as the dielectric thickness, can result in the excitation of more surface waves. Now, let us assume an array of dipoles with the element spacing of $a = b = 0.5\lambda$, dipole length of $L = 0.39\lambda$, dipole width of $W = 0.002\lambda$ and a substrate thickness and relative permittivity of $d = 0.19\lambda$ and $\epsilon_r = 2.55$, respectively.

The reflection coefficient of the array in E- ($\phi = 0$), H- ($\phi = 90$) and D-plane ($\phi = 45$) are shown in Fig. 3.3(a). The unity of the reflection coefficient in E-plane at $\theta = 45.8°$ shows the presence of the surface wave scan blindness. As explained, the scan blindness occurs when

$$(\beta_{sw}/k_0)^2 = (k_x/k_0)^2 + (k_y/k_0)^2 = (\frac{m}{a/\lambda} + \boldsymbol{u})^2 + (\frac{n}{b/\lambda} + \boldsymbol{v})^2. \tag{3.10}$$

By finding β_{sw} from Fig. 3.2 (a), two solutions can be found in the principle planes

$$\begin{array}{llll} (a) & m = -1, & n = 0, & \boldsymbol{u} = 0.717, \quad \boldsymbol{v} = 0, \\ (b) & m = 0, & n = -1, & \boldsymbol{u} = 0, \quad \boldsymbol{v} = 0.717. \end{array} \tag{3.11}$$

However, the solution (b) occurs in H-plane ($\boldsymbol{u} = 0$) while $k_x = 0$, which cancels the TM surface wave. There are other solutions satisfying (3.10) which occur off the principle planes. A contour plot of the reflection coefficient magnitude, visualizing the existance of the scan blindness in the visible area of the $u - v$ plane, is shown

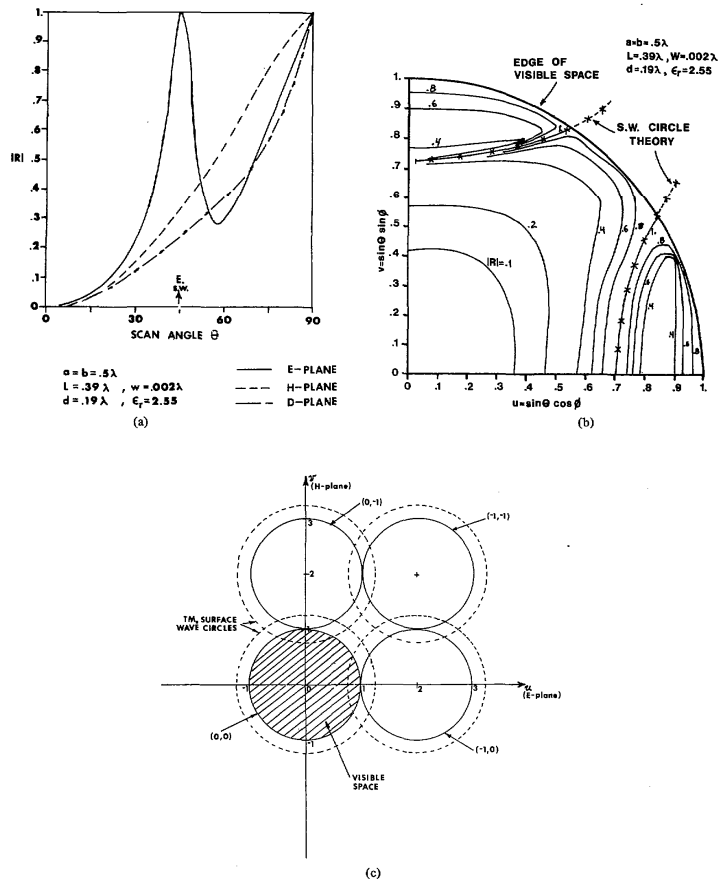

Figure 3.3: Scan characteristics of an infinite array of printed dipoles. a) Reflection coefficient magnitude at E-, H- and D-plane. b) The contour plot of reflection coefficient magnitude in the $u - v$ space and c) the surface wave circle diagram [86].

in Fig. 3.3(b). This plot shows two semicircular loci where the refection coefficient is equal to one, i.e., scan blindness. One curve starts in E-plane at $\theta = 45.8°$ and leaves the visible space at $\phi = 32.7°$ and the other one enters the visible space at $\phi = 57.3°$, approaching H-plane at $\theta = 45.8°$. However, the latter will disappear at H-plane due to the polarization cancellation mentioned earlier.

The scan blindness and the effects of the element spacing and surface wave can also be illustrated by a modified grating lobe diagram, referred to as a surface wave circle diagram, shown in Fig. 3.3(c). The solid circles are the grating lobe circle with radius one, centered at $(\boldsymbol{u} = (-m)/(a/\lambda), \boldsymbol{v} = (-n)/(b/\lambda))$. Where m and n are the Floquet mode indices. The dashed circles are centered the same as the grating lobe circles, with the radius of β_{sw}/k_0. Whenever the surface wave circles intersect the visible space, i.e., $|\boldsymbol{u}|^2 + |\boldsymbol{v}|^2 < 1$, the conditions (1) and (2) are satisfied and the scan

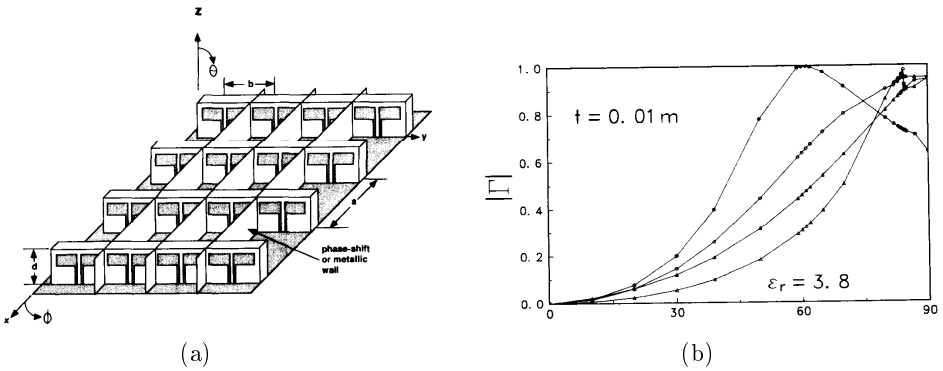

(a) (b)

Figure 3.4: a) Infinite array of dipoles on protruding susbtrate, b) Reflection coefficient versus scanning angle in E-plane [89].

blindness (unity of reflection coefficient) will happen, unless it gets canceled out due to polarization mismatch. This diagram shows that the only way to avoid blindness is to decrease the element spacing or change the substrate properties (thickness or permittivity).

3.2.2 Feed-Induced Scan Blindness

In [89], it has been shown that the coplanar feed lines in dipole arrays also introduce another blindness which affects the scan coverage of the array. As an example, an array geometry of dipoles on protruding dielectric substrate, fed by coplanar lines are shown in Fig. 3.4(a). The parameters values are $a = b = 0.5$m, $d = 0.3$m, dipole and feed line lengths are 0.375m and 0.275m, respectively. The reflection coefficient of four different arrays on a dielectric with $\epsilon_r = 3.8$ is shown in Fig. 3.4(b). From this figure, it can be seen that for dipoles with feed lines, a blindness occurs at a scan angle of 60° which does not happen in the case of dipoles without feed lines. This feed line-induced blindness can be attributed to the cancellation of the dipole radiation by the one from the coplanar feed lines, which can support a monopole type current.

It can be seen in Fig. 3.4(b) that adding the electric walls, removes the feed-induced blindness and increases the E-plane scan range, similar to the dipole array without the feed lines. Since the feed-induced blindness, similar to the surface wave blindness, is a consequence of the coupling between the adjacent elements, the electric walls will remove this blindness by isolating the neighboring elements from each other. This can also help to remove not only the feed-induced blindness, but also the blindness caused by the surface wave. Also it needs to be mentioned that introducing the feed lines can also prohibit the propagation of the surface waves.

It has been shown that changing the dielectric constant will change the location of feed-induced blindness, opposite to the one introduced by the surface wave. It means

that increasing the dielectric thickness and permitivity, will move the feed-induced blindness towards the end fire. Finally, we should mention that the effect of the feed lines gets more severe in microstrip arrays, since protruding substrate occupies only a small fraction of the element [89].

An analysis of the effect of the feed lines on the efficiency of connected arrays is presented in [90]. It is shown that feed-induced blindness is introducing other resonances caused by the common-mode propagation, which results in a strong cross-polarizing standing waves [91].

3.3 Tightly-Coupled Dipole Arrays (TCDAs)

Traditionally, the wideband arrays are designed based on designing a wideband element in isolation and then use that element in the array, hoping that the mutual coupling will not affect the element performance in the array environment. Using a fundamentally different approach to design wideband arrays, Baum showed in [92] that the interconnection of the elements in an array can introduce a continuity of the current in the array, providing low frequency performance. Later on, Tightly Coupled Dipole Arrays (TCDAs) in [23, 93], have used Wheeler's current sheet concept [94] to create current lines across the aperture. It has been shown in [23] that introducing capacitance between the ends of dipoles with small spacing, backed by a ground plane can achieve a bandwidth of $4:1$ with VSWR<2 for broadside radiation. Furthermore, a wider impedance bandwidth of $10:1$ was achieved by placing a dielectric layer over the array, known as superstrate. In the following section, we try to explain the Wheeler's current sheet, as the main concept of TCDAs.

3.3.1 Wheeler's Current Sheet

The concept of infinite array was first introduced in [95] where computations of radiating element properties in an infinite array were presented. Let's assume an infinite current sheet; electric or magnetic. Since the former can be physically realized, it will be used for the derivations.

A planar phased array of electric current sheets is shown in Fig. 3.5(a) for oblique radiation at θ_s. It is assumed that the radiation region above the array is free space and the array is backed by an open circuit reflector. The electric current sheet has a current density of I_s with uniform amplitude and is phased to radiate at θ_s. This current is associated with H_s, orthogonal to the current vector. The infinite current sheet in an area of $A = a^2$ can be assumed as equivalent to a small electric current element or electric dipole with the moment of lI, as shown in Fig. 3.5(b). The space in front of the array is partitioned by hypothetical waveguide walls determined by the imaging theory. The walls parallel to H-field are electric walls and the ones parallel to E-field are magnetic walls.

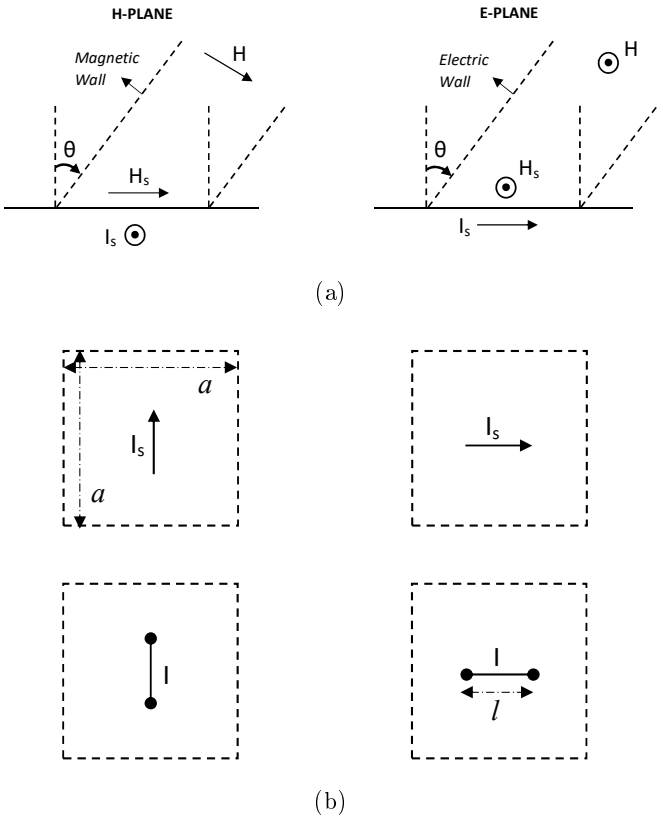

Figure 3.5: An ideal model of a planar array of an electric current sheet. a) The plane of scan, b) Plane of array, showing the element cell of current sheet and the equivalent current element [94].

The variation of the element resistance in the transmission point of view for the scanning scenario can be calculated as follow. In any plane of scan, the projection of the aperture in the beam direction is proportional to $\cos(\theta_s)$. Accordingly, this results in beamwidth proportional to $1/\cos(\theta_s)$. On the other hand, the power in the beam is proportional to the square of the farfield function i.e., $\boldsymbol{G}^2$, in the beam direction and also the beamwidth. Therefore, the relative impedance variation due to scanning can be calculated as

$$\text{H-plane:} \qquad R/R_0 = \frac{1}{\cos(\theta_s)}(\boldsymbol{G}_m(\theta_s))^2, \tag{3.12}$$

$$\text{E-plane:} \qquad R/R_0 = \frac{1}{\cos(\theta_s)}(\boldsymbol{G}_e(\theta_s))^2, \tag{3.13}$$

where $\boldsymbol{G}_m(\theta_s)$ and $\boldsymbol{G}_e(\theta_s)$ are the farfield functions of the element in H- and E-plane,

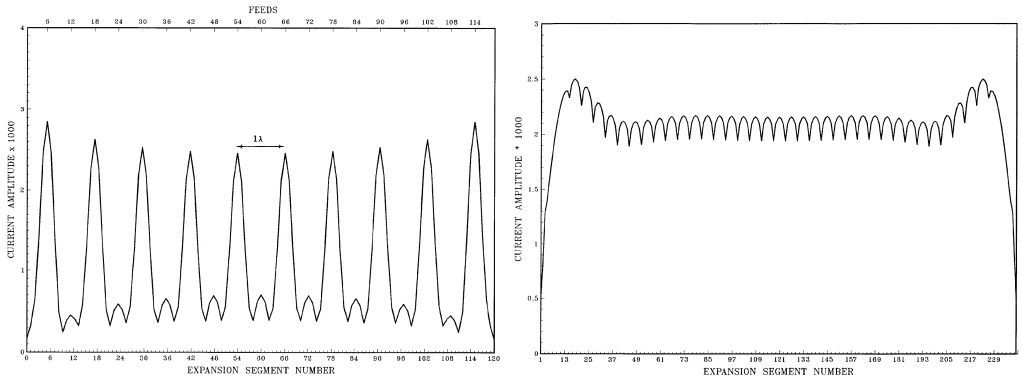

(a) (b)

Figure 3.6: The current amplitude for a 10λ linear array with feeds at a) 0.5λ for broadside and b) 0.25λ for 30° scan [96].

respectively. As an example, for an array of dipoles with doughnut-shaped element pattern, the radiation impedance will change by a factor of $cos(45) = 1.4$ (in E-plane, and $1/cos(45)$ in H-plane) for scanning to 45°.

A similar derivation can be applied for magnetic current sheet using the principle of duality. It can be seen that the impedance of the infinite current sheet is frequency independent. However, the validity of the equivalence of the infinite current sheet and the small dipole array is dependent on how closely the dipoles are spaced in the array, in terms of wavelength. In [96], the frequency/angle dependence of the current in finite interconnected arrays has been investigated. In that paper, it has been shown that for arrays of half-wave dipoles, a strong resonances will appear for the current amplitude along the array with a period of one wavelength, due to the edge currents present in finite dipole arrays. For arrays with the dipole length of $\lambda/4$ (and generally much shorter than $\lambda/2$), the current amplitude distributions are fairly constant, and the phases are well behaved for scanning, which results in an approximation to the Wheeler's current. A comparison of the current amplitude for $\lambda/2$ element spacing for broadside and $\lambda/4$ spacing for 30° scanned radiation is shown in Fig. 3.6.

Based on Eq. (3.12) and (3.13), an ideal element pattern of $\boldsymbol{G}(\theta) = \sqrt{\cos\theta}$ can provide an element resistance invariant in any scan angle. There is a simple radiating element with the same amplitude of field in all the cutting planes which offer an versatile candidate to be used as the array element. It is the so-called Huygens source which is made by the superposition of electric and magnetic dipoles [28]. Therefore, magneto-electric dipoles (MEDs) [70, 97, 98] or elements with similar characteristics are a promising option to be used in TCDAs.

Furthermore, it needs to be mentioned that in Wheeler's model, it is assumed that the current sheet has only resistance. However, the dipole array will introduce a

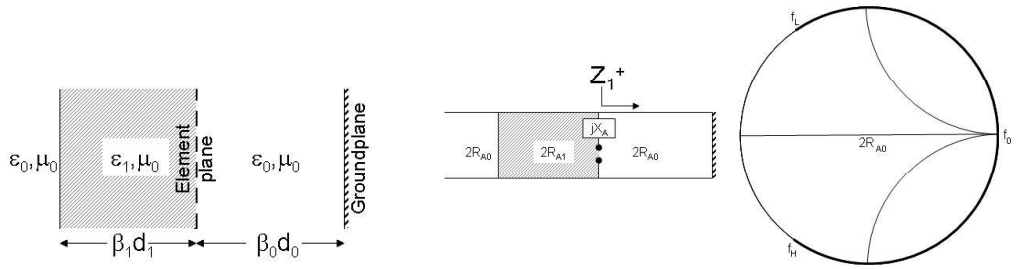

(a) (b)

Figure 3.7: a) An example of array build-up, b) the corresponding equivalent circuit and the ground plane impedance viewed from the array ports [99].

variation of the reactance which is not considered in the current sheet approximation. On the other hand, it is shown is [93, 99] that the dipole arrays backed by a ground plane can be designed in such a away to provide low reactance. Assuming short dipole elements in an infinite array, without the appearance of the grating lobe in the visible space, an equivalent circuit model for the coupled dipole above the ground plane is shown in Fig. 3.7. The substrate is air and one layer of superstrate is placed at the top of the radiating element. The variation of the impedance of the ground plane, seen from the element terminals (Z_1^+) is shown in Fig. 3.7. If we assume that the element is placed $\lambda/4$ above the ground plane at f_0, the ground plane impedance rotates along the edges of the Smith chart, since it is purely reactive. For the frequencies below f_0, this impedance is inductive and for the frequencies above f_0 it appears as capacitive. Since the reactance of dipole changes in an opposite manner, it can be used to counteract the reactance introduced by the ground plane. The addition of the capacitance between the ends of the adjacent dipoles in TCDAs is to maintain the zero reactance when the element length decreases in the tightly coupled arrays [93].

3.3.2 TCDA Examples

Various TCDAs have been proposed in the literature. An early implementation of these arrays is presented in [99]. The implementation of the inter-element coupling capacitance in a single-polarized array is shown in Fig. 3.8 (a). The array operates at $2-18$ GHz. To avoid the occurrence of the common-mode current due to the feed cables, a typical feed organizer is used for the reliable connection between the feeding and the element (See Fig. 3.8 (b)). A dual-polarized design for the same frequency range of 8×8 active elements in an array of 2664 elements is shown in Fig. 3.9. Commercially available hybrids were used to differentially excite the dipole arms. A few rows of the element around the active area is terminated to suppress the effect

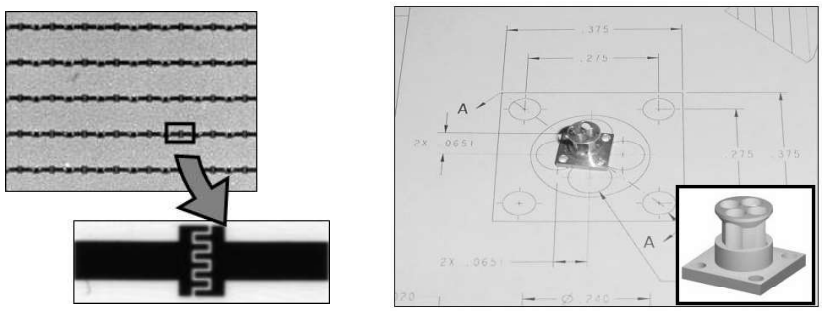

(a) (b)

Figure 3.8: a) The inter-element capacitance in a single-polarized CSA. b) The dual-polarized feed organizer [99].

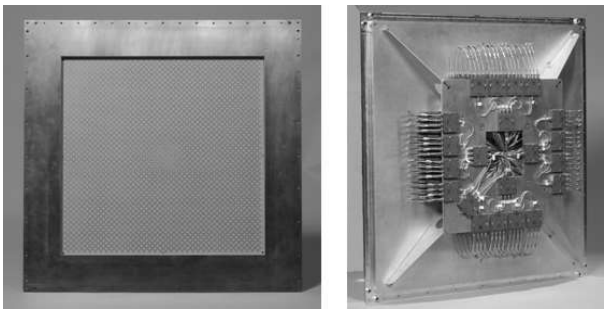

Figure 3.9: The aperture and the feed network of a 2-18 GHz dual-polarized CSA [99].

of the edge elements.

For arrays with a ground plane spacing of h, the ground plane impedance can be calculated as [100]

$$Z_{GP} = j\eta_0 \tan(\beta h), \tag{3.14}$$

where η_0 is the substrate impedance and β is the susbstrate propagation constant. Assuming air substrate, we can see that this impedance becomes zero at $f = c/2h$. Thus the array becomes short circuited, limiting the operation band. In [100], a resistive frequency selective surface (FSS) between the array and the ground plane is used to increase the bandwidth of these arrays by a factor greater than two. However, using the resistive FSS can introduce additional losses (around 4 dB) and mitigate the efficiency of the array. It is shown that a properly designed superstrate can reduce these losses to $1.1 - 1.4$ dB. The geometry of a dual-polarized unit cell of this design is shown in Fig. 3.10. The ends of the bowtie in each elements are overlapping with the ones from the adjacent elements to provide the capacitive coupling. It is shown

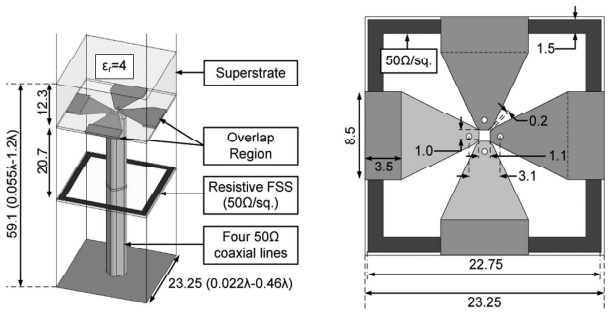

Figure 3.10: A dual polarized unit cell of a tightly coupled bowtie array with resistive FSS and superstrate [100].

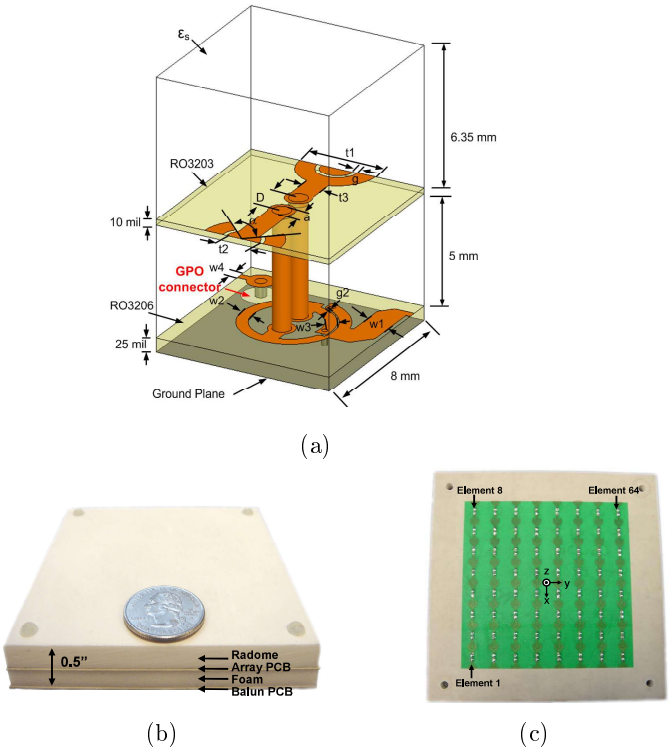

(a)

(b) (c)

Figure 3.11: a) The geometry of the unit cell and the fabricated prototype of an 8×8 array b) with and c) without radome [101].

that the array can provide a bandwidth of $21:1$ for VSWR<3 at $0.285 - 5.92$ GHz for broadside radiation.

As mentioned, a wideband TCDA requires a feed organizer and large external balun to provide the balanced feed for each element. In [7,101,102], an X-band array

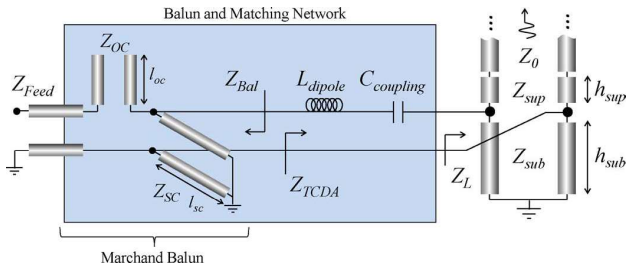

Figure 3.12: The equivalent circuit of TCDA-IB [103].

integrated with a wideband microstrip ring hybrid is designed and fabricated. In this design, due to large array input impedance (around 200-300 Ω), the element is connected to the ring with the input impedance of 100 Ω by means of a twin wire transmission line with a characteristic impedance of 136 Ω. The element and the feeding structure of this design is shown in Fig. 3.11 (a). It is shown that the array can provide an active VSWR<2 over $8-12.5$ GHz while scanning uo to 70° and 60° at E- and H-plane, respectively. A fabricated prototype of an 8×8 array using this element is shown in Fig. 3.11 (b) and (c).

To maintain the wideband characteristics of the TCDAs, a wideband balun which can be implemented in a compact volume is needed. Printed Marchand baluns have been used with dipoles in [77,103], but yield reduced overall bandwidth. However, this degradation in the impedance can be mitigated by applying a reactance cancellation technique for the array and the balun, similar to Vivaldi arrays [104]. This has been done in [105, 106], when the balun is considered as part of the impedance matching network for the arrays, in so-called TCDAs with integrated balun (TCDA-IB). The equivalent circuit model for TCDA-IB is shown in Fig. 3.12. It can be said that the addition of the balun, increases the overall order of the matching network which can help to increase the impedance bandwidth.

The unit cell of the TCDA-IB is illustrated in Fig. 3.13. As can be seen, two half elements, each comprised of the dipole and the balun are used to eliminate the need for a wideband 50Ω to 200Ω impedance transformer, since its implementation in a limited space is challenging. In order to prevent the loop resonance from one balun to another, a Wilkinson power divider is used to provide the isolation between the two connected baluns. The TCDA-IB can achieve $7.35:1$ ($0.68-5$ GHz) bandwidth for VSWR<2.65, while scanning up to 45°. An 8×8 prototype of the array is shown in Fig. 3.14. The dipole arms on the edges are extended as a way to terminate elements on the side [107].

Despite providing wideband characteristics, above mentioned TCDAs face the manufacturing and assembly complication especially at higher frequencies. Thus, fully ultrawideband modular arrays (PUMAs) are proposed in [24, 108]. These arrays

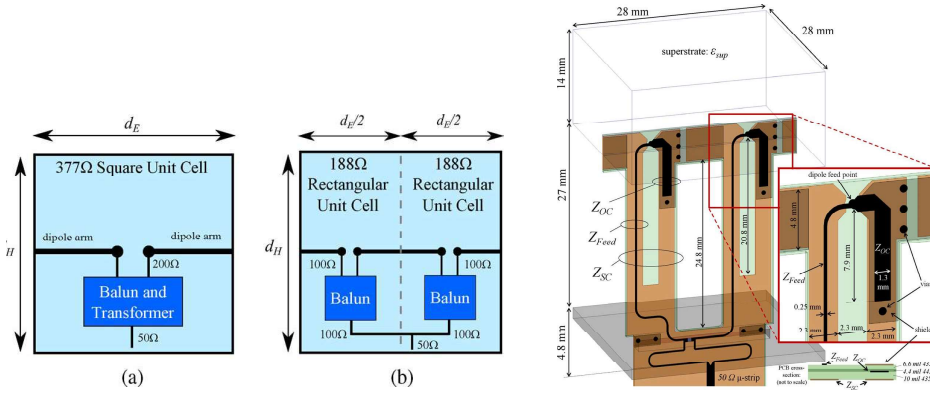

Figure 3.13: a) The illustration of the half element b) the unit cell of TCDA-IB [103].

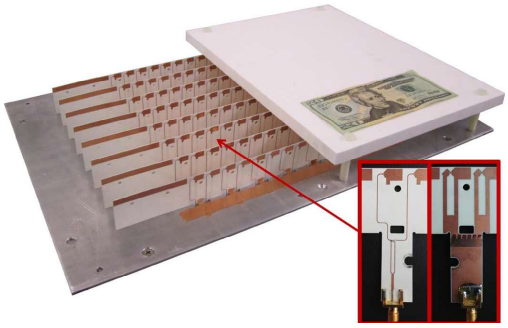

Figure 3.14: An 8×8 prototype of TCDA-IB [103].

can be fabricated with standard multilayer PCB technology. The feeding in these arrays is unbalanced and integrated with the antenna by means of plated vias. A unit cell of a dual-polarized PUMA array is shown in Fig. 3.12(a) and (b). It has been shown that the array can provide a relative bandwidth of $5:1$ ($1.06-5.3$ GHz), while scanning up to $45°$ in all planes. A fabricated prototype of 16×16 dual-polarized PUMA, operating over $7-21$ GHz ($3:1$ bandwidth) is shown in Fig. 3.12(c).

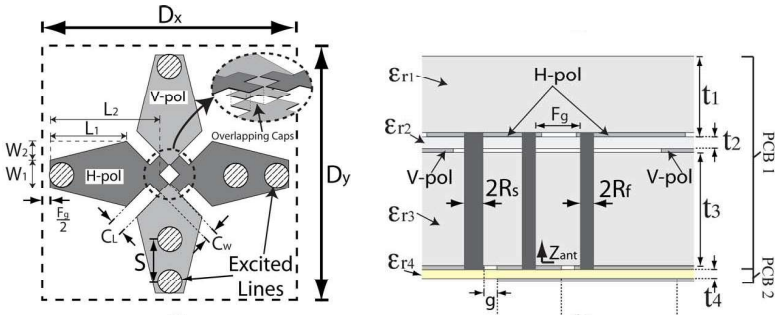

(a) (b)

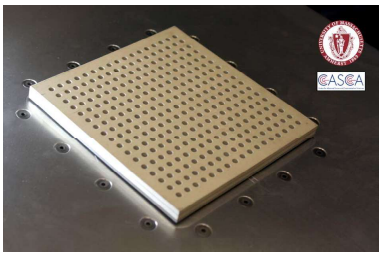

(c)

Figure 3.15: a) Top view and b) the cross sectional view of a $5:1$ dual-polarized unit cell of PUMA array [24]. c) a 16×16 prototype of a $3:1$ dual-polarized PUMA array [108].

Chapter 4

Contributions and Future Work

In the previous chapters, we presented a brief introduction to clarify the background needed for the following articles. In this chapter, a brief summary of the papers appended in Part II will be presented. Possible future work directions are also discussed below.

Paper A: Improvement of an Octave Bandwidth Bowtie Antenna Design Based on The Analysis of a MIMO Efficiency Metric in Random-LOS

In this paper, we present a new improved design of the self-grounded bowtie antenna in a 2-port realization. We put emphasis on a novel system throughput performance characterization based on the analysis of a MIMO efficiency metric in Random-LoS. Also, we identify the polarization orthogonality and the power imbalance of the 2-bitstreams as the two main factors contributing to MIMO performance degradation in Random-LoS. The antenna achieves good MIMO efficiency over an octave bandwidth, i.e., 1.65-3.3GHz, covering the target bandwidth 1.7-2.7GHz.

My contribution: I designed and simulated the antenna, analyzed the data and wrote the paper.

Paper B: Wideband Dual-Polarized Linear Array Antenna For Random-LOS OTA Measurement

In this paper, an 8×1 dual-polarized linear array antenna is proposed for a Random Line-of-Sight (Random-LoS) Over-The-Air (OTA) measurement system. The proposed array is dual-polarized operating over the frequency band of 1.6-2.7 GHz. A simple straightly-bent self-grounded bowtie is optimized as the array element. A compact wideband 2-port feeding network is designed and manufactured to differentially excite each element. Corrugated plates have been employed in the transverse plane of the linear array in order to achieve the same beamwidth for both polarizations

over the entire band. A prototype has been manufactured and the measured reflection coefficient is better than -10 dB. The realized gain and Half-Power Beamwidth (HPBW) of the array in transverse plane remain fairly constant over the entire band of interest.

My contribution: I designed, simulated and measured the antenna and wrote the paper.

Paper C: Semi-Omnidirectional Dual-Polarized Wideband Multiport Antennas for MIMO Applications in Random-LoS and RIMP

In this paper, we present two structures comprised of bowtie elements to resemble wideband dual-polarized omnidirectional antennas for MIMO applications. The elements are designed to have good performance in the embedded configuration. To evaluate the MIMO performance of both structures, the Probability of Detection (PoD) curves are plotted and MIMO multiplexing efficiencies are calculated. Using the real-life hypothesis, the MIMO performance evaluation is done in both Random-LoS and RIMP as the two complementary reference propagation environments.

My contribution: I designed and simulated the antenna, analyzed the data and wrote the paper.

Paper D: Fully-Planar Ultra-Wideband Tightly-Coupled Array (FPU-TCA) with Integrated Feed for Wide-Scanning Millimeter-Wave Applications

In this paper, we present a new design of a UWB planar array for mm-wave applications. The novelty of this work is to propose a fully planar antenna layout to provide large bandwidth at mm-wave frequencies, with large beam scanning capabilities. The antenna is realized using a simplified standard PCB manufacturing technique. The proposed antenna is based on TCDAs concept with an integrated feeding network. The feed structure is implemented by utilizing a simplified configuration of plated via holes.

My contribution: I designed, simulated and measured the antenna and wrote the paper.

Paper E: Tightly-Coupled Aperture-Coupled Magneto-Electric Dipole for Millimeter-Wave Phased-Array Antenna

In this paper, we propose a single-polarized wideband phased-array element for millimeter-wave applications. The element is comprised of tightly-coupled Magneto-Electric-Dipole fed by an aperture-coupled microstrip line. The integration of the radiating antenna element with the feed structure removes the need of external balun

and simplifies the manufacturing process. The simulated antenna provides 64% bandwidth of VSWR < 2 and 60% bandwidth of VSWR < 2.65 for scanning up to 45° and 60° in both E- and H-planes, respectively.

My contribution: I designed and simulated the antenna and wrote the paper.

Paper F: A Planar Dual-Polarized Ultra-Wideband Millimeter-Wave Array Antenna

In this paper, we present a dual-polarized ultra-wideband element in an infinite large array condition for planar phased array antennas in mm-wave applications. The array antenna consists of tightly-coupled bowties in a dual-offset configuration. In order to simplify the manufacturing process and eliminate the scalability limitation, a new feeding network is employed. The feeding is inspired by magneto-electric dipoles (MEDs) and planar ultra-wideband array antennas (PUMAs). Hence, the feeding is integrated with the horizontally oriented radiating bowties and removes the need for the external baluns. The simulated antenna shows relative bandwidths of $2.3:1$ and $3:1$ at VSWR$<$3, for maximum scanning angles of 60° and 45°, respectively, at both E- and H-planes.

My contribution: I designed and simulated the antenna and wrote the paper.

4.1 Future Work

4.1.1 OTA Evaluation and Considerations

Although 5G systems have attracted much attention in the past few years and mm-waves are believed to be the next generation for wireless communication, previous generations operating at lower frequencies are still needed to be used as a guarantee to maintain a minimum connectivity. Therefore, the design and the evaluation of the performance of the antennas based on a characterization method which relates the classical methods to MIMO OTA testing becomes important. In this thesis, we have tried to explain two extreme environments, i.e. the Rich Isotropic Multipath (RIMP) and the pure Random-LoS. Then we have defined MIMO efficiency as a figure of merit to evaluate the MIMO system performance in these two so-called edge environments. However, the calculation of MIMO efficiency can be further expanded as a function of different factors as

$$\eta_{\text{MIMO}} = \text{f}(B_p, \sigma_{amp}), \tag{4.1}$$

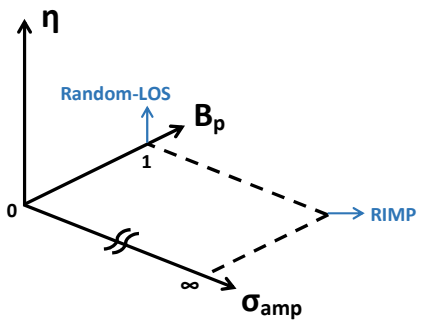

Figure 4.1: MIMO efficiency versus B_p and σ_{amp} at one given frequency over one specific coverage.

where $B_p = \frac{min(P_\theta, P_\phi)}{max(P_\theta, P_\phi)}$, ranging over $[0, 1]$ where $B_p = 1$ corresponds to same amplitude for both incoming waves polarizations and $B_p = 0$ implies that the incoming waves have only one linear polarization. σ_{amp} defines the standard deviation of a normal distribution of incoming waves. $\sigma_{amp} = 0$ corresponds to one incoming wave for each realization and $\sigma_{amp} = \infty$ is when incoming waves have a uniform distribution in terms of AoA over the desired coverage. An illustration of MIMO efficiency versus these two factors for one frequency and over one specific coverage is shown in Fig. 4.1.

One can see that the RIMP environment corresponds to $B_p = 1$ and $\sigma_{amp} = \infty$ and Random-LoS happens when $B_p = 1$ and $\sigma_{amp} = 0$. It is worthwhile to mention that a similar characterization method can be used for the embedded pattern of the beam steering phased array antenna to evaluate and further improve their MIMO performance.

4.1.2 Wideband Wide-Scanning Phased Arrays for mm-Wave 5G Base Stations

In this thesis, we have suggested some wideband wide-scanning array antenna designs for the mm-wave base station application and one prototype of a linearly-polarized antenna has been manufactured and measured. As the continuation of the antenna element designs, a simplified version of a dual-polarized element has been designed and ordered for the manufacturing. The geometry of the element has been shown in Fig. 4.2.

Also we have planned to evaluate the performance of the antenna integrated with the active circuitry in the transmit and receive modes. The block digram and the chip photograph of an integrated transmit phased array implemented by cascading the phase shifters, VGAs and four 1×4 subarrays is shown in Fig. 4.3 and Fig. 4.4,

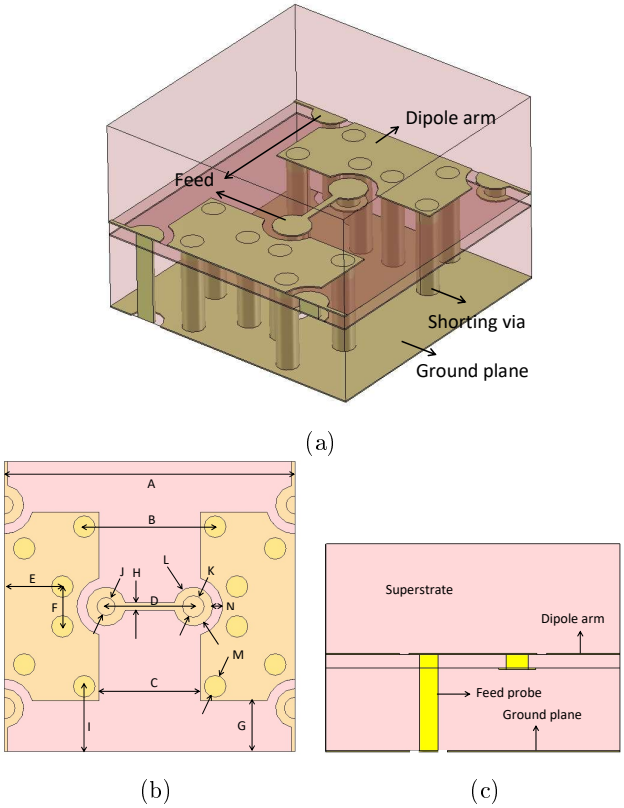

Figure 4.2: The geometry of the proposed dual polarized unit cell. a) 3D view of the element, b) the radiating (first) layer showing dipol arms and horizontal part of the feed c) the cross sectional view illustrating the gamma-shaped feed probe.

respectively. Also for the receive mode, we are trying to evaluate the element performance by its integration with ultra low power VCSELs due to their small volume and low power consumption. The block diagram of the optoelectronic receiver consist of the embedded element, LNA and VCSEL is illustrated in Fig. 4.5.

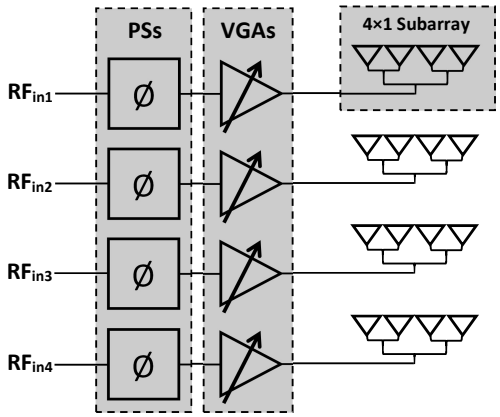

Figure 4.3: The block diagram of the transmitter phased array.

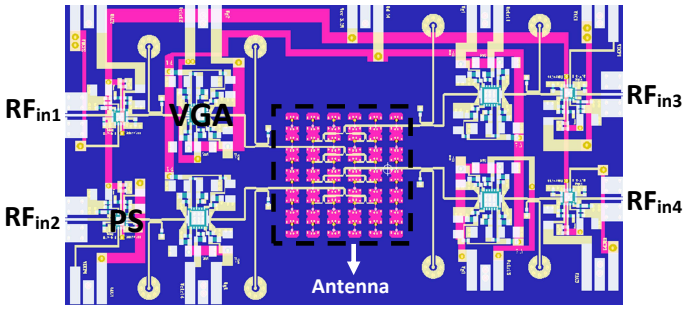

Figure 4.4: The integrated transmitter phased array.

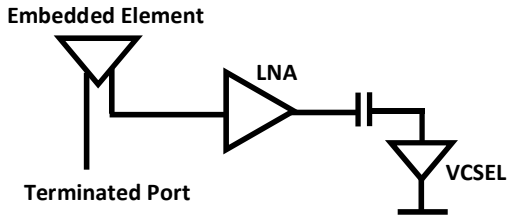

Figure 4.5: The block diagram of the receiver consist of dual-polarized embedded element, LNA and VCSEL.

References

[1] O. Teyeb, G. Wikström, M. Stattin, T. Cheng, S. Faxér, and H. Do, "Evolving LTE to fit the 5G future," *Ericsson technology review*, vol. 1, pp. 1–16, 2017.

[2] M. Series, "IMT vision framework and overall objectives of the future development of IMT for 2020 and beyond," *Recommendation ITU*, pp. 2083–0, 2015.

[3] J. Krause, "Study on scenarios and requirements for next generation access technology," 3GPP TR 38.913, Sept, Tech. Rep., 2016.

[4] A. De La Oliva, X. C. Pérez, A. Azcorra, A. Di Giglio, F. Cavaliere, D. Tiegelbekkers, J. Lessmann, T. Haustein, A. Mourad, and P. Iovanna, "Xhaul: toward an integrated fronthaul/backhaul architecture in 5G networks," *IEEE Wireless Communications*, vol. 22, no. 5, pp. 32–40, 2015.

[5] A. Checko, "Cloud RAN fronthaul options, benefits and challenges," *Presentation given in the iJOIN Winter School, Bremen, Germany*, 2015.

[6] "5G explained - how 5G works," Tech. Rep.

[7] J. A. Kasemodel, C.-C. Chen, and J. L. Volakis, "Wideband planar array with integrated feed and matching network for wide-angle scanning," *IEEE Transactions on Antennas and Propagation*, vol. 61, no. 9, pp. 4528–4537, 2013.

[8] "Spectrum for 4G and 5G," Qualcomm Technologies, Inc., Dec, Tech. Rep., 2017.

[9] W. Fan, X. Carreno, P. Kyosti, J. O. Nielsen, and G. F. Pedersen, "Over-the-air testing of MIMO-capable terminals: Evaluation of multiple-antenna systems in realistic multipath propagation environments using an OTA method," *IEEE Vehicular Technology Magazine*, vol. 10, no. 2, pp. 38–46, 2015.

[10] 3GPP, "Measurement of radiated performance for Multiple Input Multiple Output (MIMO) and multi-antenna reception for hith speed packet access (HSPA) and LTE terminals," *Tech. Rep. 37.976*, vol. 11.0.0, 2012.

References

[11] A. Hussain, P. S. Kildal, and A. A. Glazunov, "Interpreting the total isotropic sensitivity and diversity gain of LTE-enabled wireless devices from over-the-air throughput measurements in reverberation chambers," *IEEE Access*, vol. 3, pp. 131–145, 2015.

[12] A. Goldsmith, *Wireless communications*. Cambridge university press, 2005.

[13] P.-S. Kildal and J. Carlsson, "New approach to OTA testing: RIMP and pure-LOS reference environments and a hypothesis," in *7th European Conference on Antennas and Propagation (EuCAP)*, 2013, pp. 315–318.

[14] P.-S. Kildal, A. A. Glazunov, J. Carlsson, and A. Majidzadeh, "Cost-effective measurement setups for testing wireless communication to vehicles in reverberation chambers and anechoic chambers," in *IEEE Conference on Antenna Measurements and Applications (CAMA)*, 2014, pp. 1–4.

[15] A. A. Glazunov, P.-S. Kildal, and M. S. Kildal, "Devising a horizontal chamber array for automotive OTA tests in random line-of-sight," in *International Symposium on Antennas and Propagation (ISAP)*, 2015, pp. 1–4.

[16] P.-S. Kildal and K. Rosengren, "Correlation and capacity of MIMO systems and mutual coupling, radiation efficiency, and diversity gain of their antennas: simulations and measurements in a reverberation chamber," *IEEE Communications Magazine*, vol. 42, no. 12, pp. 104–112, 2004.

[17] X. Chen, P.-S. Kildal, and M. Gustafsson, "Characterization of implemented algorithm for MIMO spatial multiplexing in reverberation chamber," *IEEE Transactions on Antennas and Propagation*, vol. 61, no. 8, pp. 4400–4404, 2013.

[18] P.-S. Kildal, "Rethinking the wireless channel for OTA testing and network optimization by including user statistics: RIMP, pure-LOS, throughput and detection probability," in *International Symposium on Antennas and Propagation (ISAP)*, 2013.

[19] M. Andersson, A. Wolfgang, C. Orlenius, and J. Carlsson, "Measuring performance of 3GPP LTE terminals and small base stations in reverberation chambers," *Long Term Evolution: 3GPP LTE Radio and Cellular Technology*, 2009.

[20] P.-S. Kildal, A. Hussain, X. Chen, C. Orlenius, A. Skårbratt, J. Åsberg, T. Svensson, and T. Eriksson, "Threshold receiver model for throughput of wireless devices with MIMO and frequency diversity measured in reverberation chamber," *Antennas and Wireless Propagation Letters, IEEE*, vol. 10, pp. 1201–1204, 2011.

[21] J. G. Andrews, S. Buzzi, W. Choi, S. V. Hanly, A. Lozano, A. C. Soong, and J. C. Zhang, "What will 5G be?" *IEEE Journal on selected areas in communications*, vol. 32, no. 6, pp. 1065–1082, 2014.

[22] S. S. Holland and M. N. Vouvakis, "The banyan tree antenna array," *IEEE Transactions on Antennas and Propagation*, vol. 59, no. 11, pp. 4060–4070, 2011.

[23] B. Munk, R. Taylor, T. Durharn, W. Croswell, B. Pigon, R. Boozer, S. Brown, M. Jones, J. Pryor, S. Ortiz *et al.*, "A low-profile broadband phased array antenna," in *Antennas and Propagation Society International Symposium*, vol. 2, 2003, pp. 448–451.

[24] S. S. Holland and M. N. Vouvakis, "The planar ultrawideband modular antenna (PUMA) array," *IEEE Transactions on Antennas and Propagation*, vol. 60, no. 1, pp. 130–140, 2012.

[25] Y. P. Zhang, M. Sun, and L. Guo, "On-chip antennas for 60-GHz radios in silicon technology," *IEEE Transactions on Electron Devices*, vol. 52, no. 7, pp. 1664–1668, 2005.

[26] A. E. Lamminen, J. Saily, and A. R. Vimpari, "60-GHz patch antennas and arrays on LTCC with embedded-cavity substrates," *IEEE Transactions on Antennas and Propagation*, vol. 56, no. 9, pp. 2865–2874, 2008.

[27] M. Rumney, R. Pirkl, M. H. Landmann, and D. A. Sanchez-Hernandez, "MIMO over-the-air research, development, and testing," *International Journal of Antennas and Propagation*, 2012.

[28] P.-S. Kildal, *Foundations of Antenna Engineering: A Unified Approach for Line-Of-Sight and Multipath.* textbook published by Kildal Antenn AB, Gothenburg, Sweden, 2015 (free to download from www.kildal.se).

[29] A. Sibille and M. Mellah, "A statistical model of handsets effective gain accounting for user influence and local propagation," in *Proceedings of the Fourth European Conference on Antennas and Propagation (EuCAP)*, 2010, pp. 1–4.

[30] P.-S. Kildal, C. Orlenius, and J. Carlsson, "OTA testing in multipath of antennas and wireless devices with MIMO and OFDM," *Proceedings of the IEEE*, vol. 100, no. 7, pp. 2145–2157, 2012.

[31] M. Bäckström, O. Lundén, and P.-S. Kildal, "Reverberation chambers for emc susceptibility and emission analyses," *Review of Radio Science 1999-2002*, pp. 429–452, 2002.

[32] D. A. Hill, M. T. Ma, A. R. Ondrejka, B. F. Riddle, M. Crawford, and R. T. Johnk, "Aperture excitation of electrically large, lossy cavities," *IEEE Transactions on Electromagnetic Compatibility*, vol. 36, no. 3, pp. 169–178, 1994.

[33] J. G. Kostas and B. Boverie, "Statistical model for a mode-stirred chamber," *IEEE Transactions on Electromagnetic Compatibility*, vol. 33, no. 4, pp. 366–370, 1991.

[34] K. Rosengren and P.-S. Kildal, "Radiation efficiency, correlation, diversity gain and capacity of a six-monopole antenna array for a MIMO system: theory, simulation and measurement in reverberation chamber," *IEE Proceedings Microwaves, Antennas and Propagation*, vol. 152, no. 1, pp. 7–16, 2005.

[35] C. Orlenius, P.-S. Kildal, and G. Poilasne, "Measurements of total isotropic sensitivity and average fading sensitivity of cdma phones in reverberation chamber," in *Antennas and Propagation Society International Symposium*, vol. 1, 2005, pp. 409–412.

[36] O. Delangre, P. De Doncker, M. Lienard, and P. Degauque, "Delay spread and coherence bandwidth in reverberation chamber," *Electronics letters*, vol. 44, no. 5, pp. 328–329, 2008.

[37] X. Chen, P.-S. Kildal, C. Orlenius, and J. Carlsson, "Channel sounding of loaded reverberation chamber for over-the-air testing of wireless devices: Coherence bandwidth versus average mode bandwidth and delay spread," *IEEE Antennas and Wireless Propagation Letters*, vol. 8, pp. 678–681, 2009.

[38] K. Karlsson, X. Chen, P.-S. Kildal, and J. Carlsson, "Doppler spread in reverberation chamber predicted from measurements during step-wise stationary stirring," *IEEE Antennas and Wireless Propagation Letters*, vol. 9, pp. 497–500, 2010.

[39] X. Chen, P.-S. Kildal, and J. Carlsson, "Determination of maximum doppler shift in reverberation chamber using level crossing rate," in *Proceedings of the 5th European Conference on Antennas and Propagation (EUCAP)*, 2011, pp. 62–65.

[40] G. Alfano and A. De Maio, "Sum of squared shadowed-rice random variables and its application to communication systems performance prediction," *IEEE Transactions on Wireless Communications*, vol. 6, no. 10, 2007.

[41] M. Godavarti, T. L. Marzetta, and S. Shamai, "Capacity of a mobile multiple-antenna wireless link with isotropically random rician fading," *IEEE Transactions on Information Theory*, vol. 49, no. 12, pp. 3330–3334, 2003.

[42] M. S. Kildal, J. Kvarnstrand, J. Carlsson, A. Majidzadeh, P.-S. Kildal *et al.*, "Initial measured OTA throughput of 4G LTE communication to cars with roof-mounted antennas in 2D random-LOS," in *International Symposium on Antennas and Propagation (ISAP)*, 2015, pp. 1–4.

[43] M. S. Kildal, J. Carlsson, J. Kvarnstrand, A. Majidzadeh, P.-S. Kildal *et al.*, "Measured probabilities of detection for 1-and 2 bitstreams of 2-port car-roof antenna in RIMP and random-LOS," in *10th European Conference on Antennas and Propagation (EuCAP)*, 2016, pp. 1–5.

[44] H. Q. Ngo, E. G. Larsson, and T. L. Marzetta, "Aspects of favorable propagation in massive MIMO," in *Proceedings of the 22nd European Signal Processing Conference (EUSIPCO)*, 2014, pp. 76–80.

[45] X. Gao, O. Edfors, F. Rusek, and F. Tufvesson, "Massive MIMO performance evaluation based on measured propagation data," *IEEE Transactions on Wireless Communications*, vol. 14, no. 7, pp. 3899–3911, 2015.

[46] T. Ingason and H. Liu, "Line-of-sight MIMO for microwave links-adaptive dual polarized and spatially separated systems," 2009.

[47] P.-S. Kildal, K. Rosengren, J. Byun, and J. Lee, "Definition of effective diversity gain and how to measure it in a reverberation chamber," *Microwave and Optical Technology Letters*, vol. 34, no. 1, pp. 56–59, 2002.

[48] P.-S. Kildal, U. Carlberg, and J. Carlsson, "Definition of antenna diversity gain in user-distributed 3D-random line-of-sight," *J. Electromagn. Eng. Sci.*, vol. 13, no. 2, pp. 86–92, 2013.

[49] P.-S. Kildal, X. Chen, M. Gustafsson, and Z. Shen, "MIMO characterization on system level of 5G microbase stations subject to randomness in LOS," *Access, IEEE*, vol. 2, pp. 1064–1077, 2014.

[50] A. Razavi, A. A. Glazunov, P.-S. Kildal, and J. Yang, "Characterizing polarization-MIMO antennas in random-LOS propagation channels," *IEEE Access*, vol. 4, pp. 10 067–10 075, 2016.

[51] S. M. Moghaddam, A. A. Glazunov, P.-S. Kildal, J. Yang, and M. Gustafsson, "Improvement of an octave bandwidth bowtie antenna design based on the analysis of a mimo efficiency metric in random-los," *Microwave and Optical Technology Letters*, vol. 59, no. 6, pp. 1229–1233, 2017.

[52] S. M. Moghaddam, A. A. Glazunov, J. Yang, M. Gustafsson, and P.-S. Kildal, "Comparison of 2-bitstream polarization-MIMO performance of 2 and 4-port bowtie antennas for LTE in random-LOS," in *International Symposium on Antennas and Propagation (ISAP)*, 2015, pp. 1–4.

[53] A. Paulraj, R. Nabar, and D. Gore, *Introduction to space-time wireless communications*. Cambridge university press, 2003.

[54] X. Chen, "Throughput modeling and measurement in an isotropic-scattering reverberation chamber," *IEEE Transactions on Antennas and Propagation*, vol. 62, no. 4, pp. 2130–2139, 2014.

[55] N. Jamaly, P.-S. Kildal, and J. Carlsson, "Compact formulas for diversity gain of two-port antennas," *IEEE Antennas and Wireless Propagation Letters*, vol. 9, pp. 970–973, 2010.

[56] J. F. Valenzuela-Valdés, M. A. García-Fernández, A. M. Martínez-González, and D. A. Sánchez-Hernández, "Evaluation of true polarization diversity for MIMO systems," *IEEE Transactions on Antennas and Propagation*, vol. 57, no. 9, pp. 2746–2755, 2009.

[57] P. G. Elliot, E. N. Rosario, R. J. Davis, and A. E. Rzhanov, "MIMO polarization diversity antenna with ultra-wide bandwidth and small size," in *Phased Array Systems and Technology (ARRAY), 2010 IEEE International Symposium on*, 2010, pp. 559–566.

[58] S. Gao, L. Li, M. Leong, and T. Yeo, "A broad-band dual-polarized microstrip patch antenna with aperture coupling," *IEEE Transactions on Antennas and Propagation*, vol. 51, no. 4, pp. 898–900, 2003.

[59] K.-L. Wong and T.-W. Chiou, "Finite ground plane effects on broad-band dual polarized patch antenna properties," *IEEE Transactions on Antennas and Propagation*, vol. 51, no. 4, pp. 903–904, 2003.

[60] ——, "Broadband dual-polarized patch antennas fed by capacitively coupled feed and slot-coupled feed," *IEEE Transactions on Antennas and Propagation*, vol. 50, no. 3, pp. 346–351, 2002.

[61] H. Wong, K.-L. Lau, and K.-M. Luk, "Design of dual-polarized l-probe patch antenna arrays with high isolation," *IEEE Transactions on Antennas and Propagation*, vol. 52, no. 1, pp. 45–52, 2004.

[62] Y.-X. Guo, K.-M. Luk, and K.-F. Lee, "Broadband dual polarization patch element for cellular-phone base stations," *IEEE Transactions on Antennas and Propagation*, vol. 50, no. 2, pp. 251–253, 2002.

[63] C. Mak, K. Luk, K. Lee, and Y. Chow, "Experimental study of a microstrip patch antenna with an l-shaped probe," *IEEE Transactions on Antennas and Propagation*, vol. 48, no. 5, pp. 777–783, 2000.

[64] Y.-H. Huang, Q. Wu, and Q.-Z. Liu, "Broadband dual-polarised antenna with high isolation for wireless communication," *Electronics Letters*, vol. 45, no. 14, pp. 714–715, 2009.

[65] Z. Bao, Z. Nie, and X. Zong, "A novel broadband dual-polarization antenna utilizing strong mutual coupling," *IEEE Transactions on Antennas and Propagation*, vol. 62, no. 1, pp. 450–454, 2014.

[66] B. Li, Y.-Z. Yin, W. Hu, Y. Ding, and Y. Zhao, "Wideband dual-polarized patch antenna with low cross polarization and high isolation," *IEEE Antennas and Wireless Propagation Letters*, vol. 11, pp. 427–430, 2012.

[67] Y. Cui, R. Li, and H. Fu, "A broadband dual-polarized planar antenna for 2G/3G/LTE base stations," *IEEE Transactions on Antennas and Propagation*, vol. 62, no. 9, pp. 4836–4840, 2014.

[68] L. Siu, H. Wong, and K.-M. Luk, "A dual-polarized magneto-electric dipole with dielectric loading," *IEEE Transactions on Antennas and Propagation*, vol. 57, no. 3, pp. 616–623, 2009.

[69] H. Wong and K. Luk, "Design of a magneto-electric dipole element for mobile communication base station antennas," *ZTE Communications*, vol. 9, no. 2, pp. 20–26, 2011.

[70] B. Q. Wu and K.-M. Luk, "A broadband dual-polarized magneto-electric dipole antenna with simple feeds," *IEEE Antennas and Wireless Propagation Letters*, vol. 8, pp. 60–63, 2009.

[71] T.-H. Chio and D. H. Schaubert, "Parameter study and design of wide-band widescan dual-polarized tapered slot antenna arrays," *IEEE Transactions on Antennas and Propagation*, vol. 48, no. 6, pp. 879–886, 2000.

[72] G. Adamiuk, T. Zwick, and W. Wiesbeck, "Compact, dual-polarized uwb-antenna, embedded in a dielectric," *IEEE Transactions on Antennas and Propagation*, vol. 58, no. 2, pp. 279–286, 2010.

[73] Y.-X. Guo, K.-W. Khoo, and L. C. Ong, "Wideband dual-polarized patch antenna with broadband baluns," *IEEE Transactions on Antennas and Propagation*, vol. 55, no. 1, pp. 78–83, 2007.

[74] Y.-G. Kim, D.-S. Woo, K. W. Kim, and Y.-K. Cho, "A new ultra-wideband microstrip-to-cps transition," in *IEEE/MTT-S International Microwave Symposium*, 2007, pp. 1563–1566.

[75] J. Chramiec and B. Janiczak, "Design of impedance-transforming microstrip-balanced stripline tapered transitions," *Electronics Letters*, vol. 29, no. 1, pp. 3–4, 1993.

[76] Z.-Y. Zhang and K. Wu, "A broadband substrate integrated waveguide (siw) planar balun," *IEEE Microwave and Wireless Components Letters*, vol. 17, no. 12, pp. 843–845, 2007.

[77] R. Li, T. Wu, B. Pan, K. Lim, J. Laskar, and M. M. Tentzeris, "Equivalent-circuit analysis of a broadband printed dipole with adjusted integrated balun and an array for base station applications," *IEEE Transactions on Antennas and Propagation*, vol. 57, no. 7, pp. 2180–2184, 2009.

[78] H. Ta, A. Stameroff, and A.-V. Pham, "Development of a defected ground structure wide bandwidth balun on multilayer organic substrate," in *Asia-Pacific Microwave Conference Proceedings*, 2010, pp. 1641–1644.

[79] F. Zhu, W. Hong, J.-X. Chen, and K. Wu, "Ultra-wideband single and dual baluns based on substrate integrated coaxial line technology," *IEEE Transactions on Microwave Theory and Techniques*, vol. 60, no. 10, pp. 3062–3070, 2012.

[80] Z.-Y. Zhang, Y.-X. Guo, L. C. Ong, and M. Chia, "A new wide-band planar balun on a single-layer PCB," *IEEE Microwave and Wireless Components Letters*, vol. 15, no. 6, pp. 416–418, 2005.

[81] H. Okabe, C. Caloz, and T. Itoh, "A compact enhanced-bandwidth hybrid ring using an artificial lumped-element left-handed transmission-line section," *IEEE Transactions on Microwave Theory and Techniques*, vol. 52, no. 3, pp. 798–804, 2004.

[82] J. Yang and A. Kishk, "A novel low-profile compact directional ultra-wideband antenna: the self-grounded bow-tie antenna," *IEEE Transactions on Antennas and Propagation*, vol. 60, no. 3, pp. 1214–1220, 2012.

[83] H. Raza, A. Hussain, J. Yang, and P.-S. Kildal, "Wideband compact 4-port dual polarized self-grounded bowtie antenna," *IEEE Transactions on Antennas and Propagation*, vol. 62, no. 9, pp. 4468–4473, 2014.

[84] A. Razavi, A. A. Glazunov, P.-S. Kildal, and R. Maaskant, "Array-fed cylindrical reflector antenna for automotive OTA tests in random line-of-sight," in *10th European Conference on Antennas and Propagation (EuCAP)*, 2016, pp. 1–4.

[85] H. Unz, "Linear arrays with arbitrarily distributed elements," *IRE Transactions on Antennas and Propagation*, vol. 8, no. 2, pp. 222–223, 1960.

[86] D. Pozar and D. Schaubert, "Scan blindness in infinite phased arrays of printed dipoles," *IEEE Transactions on Antennas and Propagation*, vol. 32, no. 6, pp. 602–610, 1984.

[87] N. Amitay, V. Galindo, and C. P. Wu, "Theory and analysis of phased array antennas." *Theory and analysis of phased array antennas., by Amitay, N.; Galindo, V.; Wu, CP. Chichester (UK): John Wiley & Sons, 480 p.*, 1972.

[88] G. H. Knittel, A. Hessel, and A. A. Oliner, "Element pattern nulls in phased arrays and their relation to guided waves," *Proceedings of the IEEE*, vol. 56, no. 11, pp. 1822–1836, 1968.

[89] J.-P. Bayard, D. H. Schaubert, and M. E. Cooley, "E-plane scan performance of infinite arrays of dipoles printed on protruding dielectric substrates: Coplanar feed line and e-plane metallic wall effects," *IEEE Transactions on Antennas and Propagation*, vol. 41, no. 6, pp. 837–841, 1993.

[90] S. Hay and J. O'sullivan, "Analysis of common-mode effects in a dual-polarized planar connected-array antenna," *Radio Science*, vol. 43, no. 6, 2008.

[91] D. Cavallo, A. Neto, and G. Gerini, "PCB slot based transformers to avoid common-mode resonances in connected arrays of dipoles," *IEEE Transactions on Antennas and Propagation*, vol. 58, no. 8, pp. 2767–2771, 2010.

[92] C. E. Baum, "Transient arrays," in *Ultra-Wideband, Short-Pulse Electromagnetics 3*. Springer, 1997, pp. 129–138.

[93] B. A. Munk, *Finite antenna arrays and FSS*. John Wiley & Sons, 2003.

[94] H. Wheeler, "Simple relations derived from a phased-array antenna made of an infinite current sheet," *IEEE Transactions on Antennas and Propagation*, vol. 13, no. 4, pp. 506–514, 1965.

[95] H. A. Wheeler, "The radiation resistance of an antenna in an infinite array or waveguide," *Proceedings of the IRE*, vol. 36, no. 4, pp. 478–487, 1948.

[96] R. Hansen, "Linear connected arrays," *IEEE Antennas Wireless Propag. Lett*, vol. 3, no. 1, pp. 154–156, 2004.

[97] K.-M. Luk and H. Wong, "A new wideband unidirectional antenna element," *Int. J. Microw. Opt. Technol.*, vol. 1, no. 1, pp. 35–44, 2006.

[98] X. Cui, F. Yang, M. Gao, L. Zhou, Z. Liang, and F. Yan, "A wideband magneto-electric dipole antenna with microstrip line aperture-coupled excitation," *IEEE Transactions on Antennas and Propagation*, vol. 65, no. 12, pp. 7350–7354, 2017.

[99] M. Jones and J. Rawnick, "A new approach to broadband array design using tightly coupled elements," in *MILCOM 2007-IEEE Military Communications Conference*, 2007, pp. 1–7.

[100] W. F. Moulder, K. Sertel, and J. L. Volakis, "Superstrate-enhanced ultrawideband tightly coupled array with resistive fss," *IEEE Transactions on Antennas and Propagation*, vol. 60, no. 9, pp. 4166–4172, 2012.

[101] J. A. Kasemodel, C.-C. Chen, and J. L. Volakis, "Broadband planar wide-scan array employing tightly coupled elements and integrated balun," in *IEEE International Symposium on Phased Array Systems and Technology*, 2010, pp. 467–472.

[102] ——, "Low-cost, planar and wideband phased array with integrated balun and matching network for wide-angle scanning," in *IEEE Antennas and Propagation Society International Symposium*, 2010, pp. 1–4.

[103] P. Lindberg, E. Ojefors, Z. Barna, A. Thornell-Pers, and A. Rydberg, "Dual wideband printed dipole antenna with integrated balun," *IET microwaves, antennas and propagation*, vol. 1, no. 3, pp. 707–711, 2007.

[104] J. Shin and D. H. Schaubert, "A parameter study of stripline-fed vivaldi notch-antenna arrays," *IEEE Transactions on Antennas and Propagation*, vol. 47, no. 5, pp. 879–886, 1999.

[105] J. P. Doane, K. Sertel, and J. L. Volakis, "A 6.3 : 1 bandwidth scanning tightly coupled dipole array with co-designed compact balun," in *Proceedings of the IEEE International Symposium on Antennas and Propagation*, 2012, pp. 1–2.

[106] ——, "A wideband, wide scanning tightly coupled dipole array with integrated balun (TCDA-IB)," *IEEE Transactions on Antennas and Propagation*, vol. 61, no. 9, pp. 4538–4548, 2013.

[107] I. Tzanidis, K. Sertel, and J. L. Volakis, "Characteristic excitation taper for ultrawideband tightly coupled antenna arrays," *IEEE Transactions on Antennas and Propagation*, vol. 60, no. 4, pp. 1777–1784, 2012.

[108] S. S. Holland, D. H. Schaubert, and M. N. Vouvakis, "A 7-21 GHz dual-polarized planar ultrawideband modular antenna (PUMA) array," *IEEE Transactions on Antennas and Propagation*, vol. 60, no. 10, pp. 4589–4600, 2012.